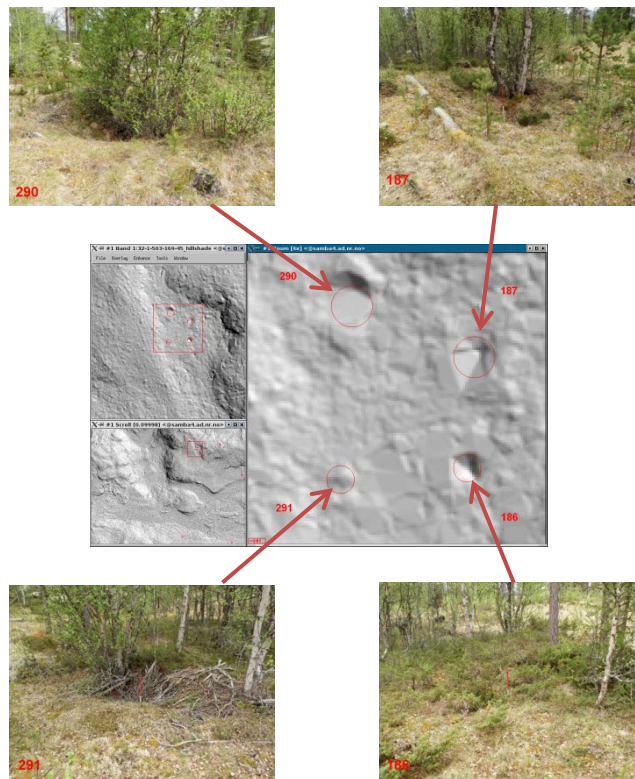


# Application of remote sensing in cultural heritage management

## Project Report 2011



**SAMBA/09/12**

**Øivind Due Trier (NR), Lars Gustavsen (NIKU), Lars Holger Pilø (OFK), Christer Tønning (VFK)**

**13 March 2012**

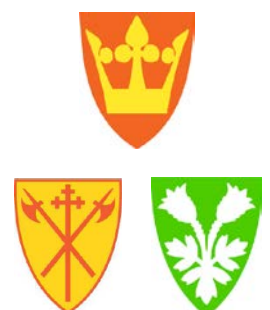
Note no

Authors

Date



UiO : Kulturhistorisk museum



## **Norsk Regnesentral**

Norsk Regnesentral (Norwegian Computing Center, NR) is a private, independent, non-profit foundation established in 1952. NR carries out contract research and development projects in the areas of information and communication technology and applied statistical modelling. The clients are a broad range of industrial, commercial and public service organizations in the national as well as the international market. Our scientific and technical capabilities are further developed in co-operation with The Research Council of Norway and key customers. The results of our projects may take the form of reports, software, prototypes, and short courses. A proof of the confidence and appreciation our clients have for us is given by the fact that most of our new contracts are signed with previous customers.

## **Front page illustration**

The central grey scale image is a hill-shaded visualisation of lidar data from Nord-Fron municipality, Norway, showing an ancient iron extraction site consisting of four charcoal burning pits. The four surrounding colour photographs are from field inspection, each photograph showing one charcoal burning pit.

<b>Title</b>	<b>Application of remote sensing in cultural heritage management – Project report 2011</b>
<b>Authors</b>	<b>Øivind Due Trier (NR), Lars Gustavsen (NIKU), Lars Holger Pilø (OFK), Christer Tonning (VFK)</b>
Quality assurance	Rune Solberg
Date	13 March 2012
Year	2012
Publication number	SAMBA/09/12

### Abstract

The project was started in 2002 with the overall aim of developing a cost-effective method for surveying and monitoring cultural heritage sites on a regional and national scale. The project focuses on the development of automated pattern recognition methods for detecting and locating cultural heritage sites.

The pattern recognition methods are included in a prototype software called *CultSearcher*. This software currently supports the following: (1) Search for crop marks and soil marks in optical satellite and aerial imagery; these marks could be levelled grave mounds. (2) Search for pits in lidar data; these pits could be pitfall traps or charcoal burning pits.

This note describes the achievements of the project during 2011. The project is funded by the Norwegian Directorate for Cultural Heritage.

In 2011, the method for automatic detection of pits in lidar data was further developed, and is now being used operationally by Oppland County as part of their cultural heritage survey work. The next step is to include automatic detection of grave mounds in lidar data in *CultSearcher*. This work has started, and will continue in 2012.

We have continued to monitor the Brunlanes and Tjølling study areas in Vestfold County with Worldview-2 satellite images. Unfortunately, a very wet summer prevented crop marks from developing in the fields. For two of the crop mark locations in 2009/2010 satellite images, archaeological field work was done, confirming the presence of circular ditches corresponding to the crop marks.

Keywords	Lidar, Worldview-2, georadar, crop marks, levelled grave mounds, pitfall traps, hunting systems, iron extraction, charcoal burning pits, pattern recognition, remote sensing.
Target group	Archaeologists, remote sensing researchers, cultural heritage management
Availability	Open
Project number	220489 CultSearcher-2011
Research field	Earth observation, archaeology
Number of pages	69
© Copyright	Norsk Regnesentral



# Contents

<b>1</b>	<b>Introduction</b> .....	<b>7</b>
<b>2</b>	<b>Semi-automatic detection of hunting systems and iron extraction sites in lidar data</b>	<b>8</b>
2.1	Introduction.....	8
2.2	Data and methods .....	9
2.2.1	Airborne lidar height measurements.....	9
2.2.2	Automatic detection of pitfall traps in lidar height images.....	11
2.3	Results.....	18
2.3.1	Automatic detection of cultural heritage pits in lidar data of Olstappen.....	18
2.3.2	Detection of pits in reduced versions of lidar data .....	25
2.3.3	Operational use in Øystre Slidre municipality, Norway.....	27
2.4	Discussion .....	30
<b>3</b>	<b>Automatic detection of grave mounds in lidar data</b> .....	<b>33</b>
<b>4</b>	<b>Acquisition of satellite imagery</b> .....	<b>36</b>
<b>5</b>	<b>Field inspection of crop marks</b> .....	<b>40</b>
5.1	Field work at Valby, Larvik, Norway – non-intrusive methods .....	40
5.2	Results, small scale archaeological excavation at Valby .....	44
5.2.1	Concluding remarks .....	49
5.3	Geophysical survey of crop marks at Store Sandnes .....	50
5.3.1	Introduction .....	51
5.3.2	Site description and survey.....	51
5.3.3	Method and instrumentation .....	52
5.3.4	Results .....	52
5.3.5	Discussion.....	55
5.3.6	Remarks.....	55
5.4	Crop mark detections pending field verification .....	57
<b>6</b>	<b>Pilot portal</b> .....	<b>62</b>
6.1	Detailed description .....	62
<b>7</b>	<b>Discussion and Conclusion</b> .....	<b>67</b>
	<b>References</b> .....	<b>68</b>



# 1 Introduction

Several Norwegian municipalities are experiencing growing pressure on agricultural and forested land for development, being it new residential areas, new mountain cabins and hotels, new highways, or other purposes. The traditional mapping of cultural heritage, mainly based on chance discovery and with inaccurate positioning, has proven inadequate for land use planning. Therefore, the Norwegian Directorate for Cultural Heritage, in cooperation with some Norwegian counties and municipalities, are investing in the development of new methods, using new technology, for a more systematic mapping of cultural heritage.

A project was started in 2002 by the Norwegian Directorate for Cultural Heritage, aiming at developing cost-effective methods for surveying and monitoring cultural heritage on a regional and national scale. During the first years, the focus was on the automatic detection of crop marks and soil marks in cereal fields in satellite and aerial images (Aurdal et al., 2006; Trier et al., 2009). Several of these detections have been confirmed to be levelled grave mounds, dating to 1500-2500 years ago.

However, methods based on optical images are of limited value in forested areas, since the archaeology tends to be obscured by the tree canopies. However, by using lidar data, the forest vegetation can be removed from the data, which makes it possible to detect archaeology in a semi-automatic fashion, provided the archaeology manifests itself as details in the digital elevation model of the lidar ground returns (Figure 1), and that these details may be described using some kind of pattern.

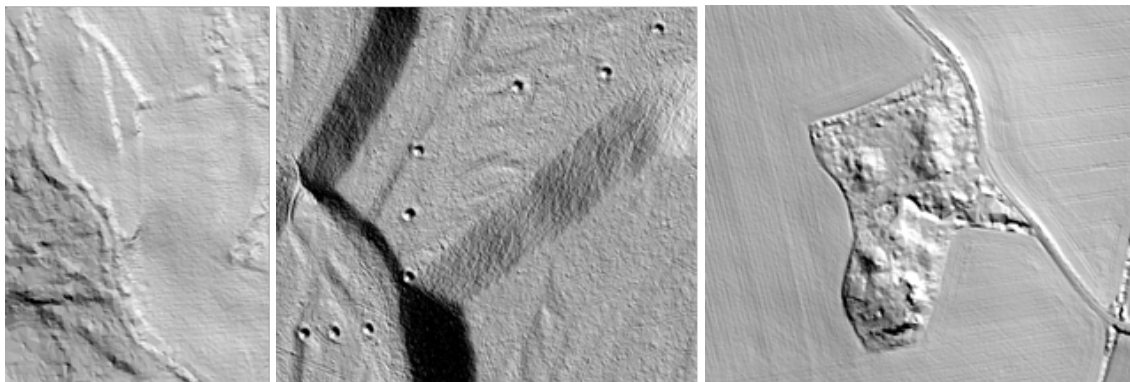


Figure 1. Lidar data from some Norwegian municipalities. Left: Kongsberg, with stone fences. Middle: Nord-Fron, with pitfall traps for deer hunting. Right: Larvik, with grave mounds.

## 2 Semi-automatic detection of hunting systems and iron extraction sites in lidar data

### 2.1 Introduction

Oppland County in Norway has a large number of ancient iron production sites and hunting systems. Today, these are manifested as pits in the ground. The iron production sites were used 1400-700 years ago, and consist of charcoal burning pits, often located in groups of four around a central oven, which can occasionally also be located as a small heap. The hunting systems were used 2000-500 years ago, and consisted of concealed pitfall traps and wooden fences, located in deer trekking routes. The fences are gone, but the pits remain. Many of the iron production sites and hunting systems are located in forested areas. The current, traditional mapping of these is relatively poor, with many individual pits missing, and poor positional accuracy of the ones that are mapped. This means that overlays of cultural heritage sites cannot be trusted when planning new highways, residential areas, cabins, etc.

Airborne laser scanning, or lidar, is a relatively new data source that allows very detailed mapping of the ground surface, even in forested areas. Recently, airborne lidar has been used for the purpose of detecting cultural heritage sites. Bewley et al. (2005) used a digital elevation model (DEM) derived from lidar height measurements to map previously unknown details of the Stonehenge World Heritage Site. The height accuracy of the lidar measurements was able to reveal details that had been previously overlooked and regarded as 'no visible surface expression'. Devereux et al. (2005, 2008) explored the possibilities of varying the sun elevation and illumination direction when hill-shading the lidar DEM, and noted that some structures may be missed by human interpretation if only one illumination direction is used. They further demonstrated that by using only the lidar pulses that were reflected by the ground, and not the lidar pulses reflected by trees, in effect removing the forest vegetation from the DEM, a very detailed elevation model of the ground was obtained. For the particular study site, more detail was apparent in the DEM than could be seen in the existing archaeological map. Hesse (2010) subtracted a smoothed version of the ground surface DEM from the original to obtain a local height model, thus enhancing local detail and suppressing the large-scale terrain. The local height model could be viewed directly as a grey scale image. It was often an advantage to view both the local height model and a hill-shade model of the original ground surface DEM to get the landscape context when doing visual interpretation. Kokalj et al. (2011) computed the sky-view factor to emphasis local detail. Hesse (2010) further noticed that some archaeological structures, such as burial mounds, can be confused with natural phenomena such as small natural hills, wood piles, and patches of low vegetation. Coluzzi et al. (2010) used full-waveform lidar to better discriminate between low vegetation and structures of archaeological interest.

Automatic detection in lidar data may either be done directly on the lidar point cloud or on a derived DEM with a suitably chosen pixel size. Sampath and Shan (2010) extracted planar surfaces directly from the point cloud to detect building roofs. Wang and Tseng (2004) used an octree subdivision of the point cloud to identify planar patches, then merging patches belonging to the same plane. To extract buildings, Rottensteiner and Briese (2002) filtered the lidar points into terrain and off-terrain points in an iterative process, resulting in a digital terrain model (DTM), which is a smoothed model of the terrain points, and a digital surface model (DSM), which is a non-smoothed model of all the lidar points. The DTM was subtracted from the DSM, resulting in a local height model. This DEM was then used for building extraction. Kwak et al. (2007) used the TerraScan software to classify lidar points into ground,

low vegetation, medium vegetation and high vegetation. The high vegetation returns were used to generate a DSM, while the ground returns gave a DTM. By subtracting the DTM from the DSM, a digital canopy model (DCM) was obtained, and individual trees were extracted from this DEM.

A paper based on this chapter will appear in *Archaeological Prospection* (Trier and Pilø, 2012).

## 2.2 Data and methods

### 2.2.1 Airborne lidar height measurements

In this study, two lidar datasets from Oppland County, Norway, have been used (Figure 2, Table 1).

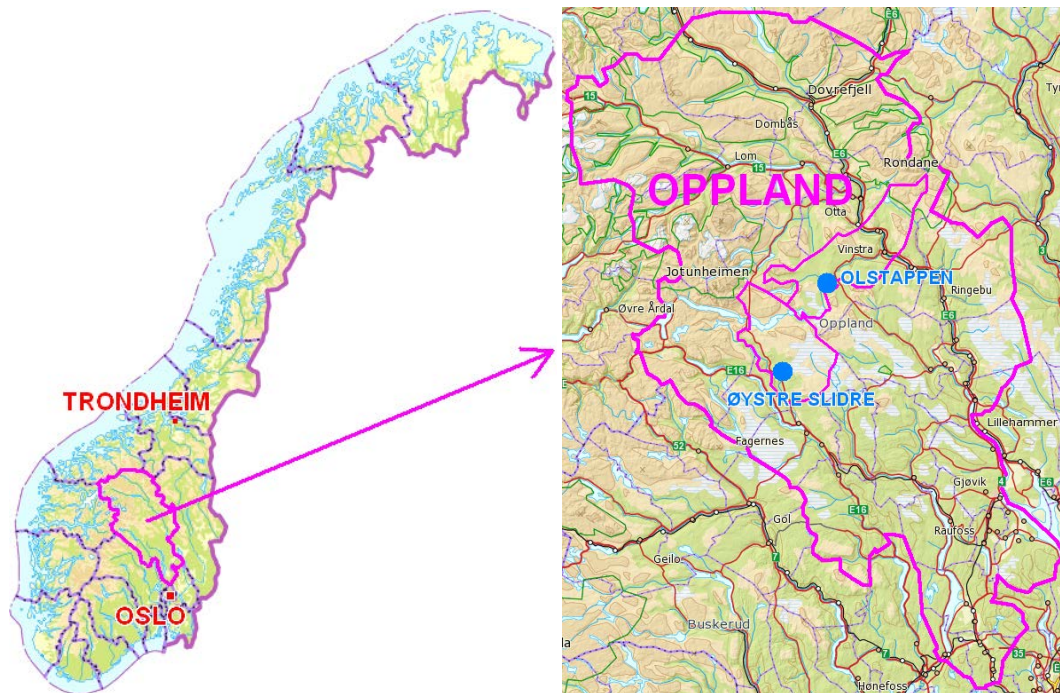


Figure 2. The two lidar data sets are located in Oppland County, Norway: Olstappen and Øystre Slidre data sets. The maps are downloaded from <http://kart.statkart.no>, copyright: Norwegian Mapping Authority.

#### 2.2.1.1 Olstappen dataset

For an area surrounding the lake Olstappen in Nord-Fron municipality, data was acquired by helicopter, with a minimum of 10 emitted laser pulses per m<sup>2</sup>. The data set covered a total area of 29.3 km<sup>2</sup>, with 7.3 ground hits per m<sup>2</sup> on average. This terrain is dominated by open pine forest, allowing a large proportion of hits from the ground. The dataset is divided into 600 m × 800 m tiles (Figure 3). This area is known to contain several systems of pitfall traps that were used in moose hunting 500-2000 years ago.

#### 2.2.1.2 Øystre Slidre dataset

For a 400 km<sup>2</sup> area in Øystre Slidre municipality, lidar data was collected in June 2011, with 5 emitted pulses per m<sup>2</sup> and 2.1 ground hits per m<sup>2</sup> on average. This area is known to contain a number of ancient iron production sites, with many visible coal burning pits. The particular choice of point density was determined from the analysis of the reduced point density datasets in Section 2.2.1.3. The Øystre Slidre data set is subdivided into 1 km by 1 km tiles, 487 in total.

Table 1. Lidar acquisition parameters.

Dataset	Olstappen, Nord-Fron	Øystre Slidre
Date	29 June 2010	4-5 June 2011
Platform	Helicopter	Aircraft
Instrument	Leica ALS50-II snr 051	Leica ALS70
Field of view	20 degrees	20 degrees
Emitted pulses per area	10/m <sup>2</sup>	5/m <sup>2</sup>
Laser wavelength	1064 nm	1064 nm
Full waveform	no	no
Pulse rate	133 kHz	267.2 kHz
Multipulse	no	enabled
Scan rate	63.8 Hz	55.4 Hz
Height above lowest terrain	650 m	
Flying altitude	1350 masl	2500-3200 masl
Flying speed	135 knots	135 knots
Number of strips	41	56
Strip overlap	20 %	20 %
Sum strip length	230 km	512 km
Mapped area	29.3km <sup>2</sup>	400km <sup>2</sup>



Figure 3. One lidar image tile from the Olstappen data set in Nord-Fron municipality, covering a 600 m × 800 m area of relatively open pine forest. The lidar height data is visualized with hill shading. 12 pitfall traps are clearly visible in the upper right part of the image.

### 2.2.1.3 Reduced point density versions of the Olstappen dataset

In order to simulate the effect of acquiring lidar data at lower point densities, reduced point density versions of the Olstappen dataset is produced as follows. For each ground reflection, a number between 0.0 and 1.0 is drawn randomly from a uniform distribution. Then, for each point sampling factor, a ground reflection is kept if the associated random number is below the sampling factor. For example, if the point sampling factor is 0.1, then only ground reflections with random numbers below 0.1 are included. For each ground reflection, the associated random number is drawn only once, so that if the ground reflection is included at a specific point sampling factor, then it is included for all higher point sampling factors as well.

20 point sampling factors were used, from 1.0 to 0.001, resulting in point sampling densities between 7.277 and 0.007 points per m<sup>2</sup> (Table 2).

Table 2. Point sampling densities, in points per square meter, for the original and the 19 reduced density versions.

Point sampling factor	1	0,9	0,8	0,7	0,6	0,5	0,4	0,3	0,25	0,2
Point sampling density	7,277	6,549	5,822	5,094	4,366	3,638	2,911	2,183	1,819	1,455
Point sampling factor	0,15	0,1	0,08	0,06	0,04	0,02	0,01	0,005	0,003	0,001
Point sampling density	1,092	0,728	0,582	0,437	0,291	0,146	0,073	0,036	0,022	0,007

## 2.2.2 Automatic detection of pitfall traps in lidar height images

### 2.2.2.1 Pre-processing of LAS files

The lidar data is available as binary data files in the LAS files format (*LAS Specification, 2011*), containing up to four returns per emitted laser pulse. Each return contains x-, y-, and z-coordinates in UTM zone 32, and a class label denoting if it is a ground, vegetation, or building point. We are only interested in the ground points, and prefer to do the detection on a regular grid (image) rather than arbitrary points. The following steps are used to convert the LAS files to a 0.2 m grid in the x-y plane with floating point height values in meters. This gives 25 grid cells per square metres, and appears to preserve all the detail of lidar point clouds with up to 10 emitted pulses per square metre.

1. Create a triangulation of all the ground returns.
2. Convert the triangulation to a digital elevation model (DEM) with 0.2 m ground resolution in the x- and y-coordinates, and floating point-valued height values in meters.

### 2.2.2.2 Detection method

The detection method uses the following main steps, similarly to the ring detection method for soil marks and crop marks in optical images (Trier *et al.*, 2009):

1. Convolve the image with templates of varying sizes. Threshold each convolution result to obtain detections.
2. Merge detections that are closer than a distance threshold, keeping the strongest detections.
3. For each detection, compute measurements that measure the deviation from an ideal model, using different measures than the convolution in step 1.

4. Remove detections that have measurement values outside prescribed intervals.
5. (Optional) Remove detections that are adjacent to roads and water courses.

#### 2.2.2.2.1 Pit templates

Each pit template in step 1 is a hemisphere with a ring edge (Figure 4). We used 12 pit templates with radii from 6 to 17 pixels, that is, 1.2 to 3.4 meters, each template having 1 pixel (0.2 m) larger radius than the next smaller.

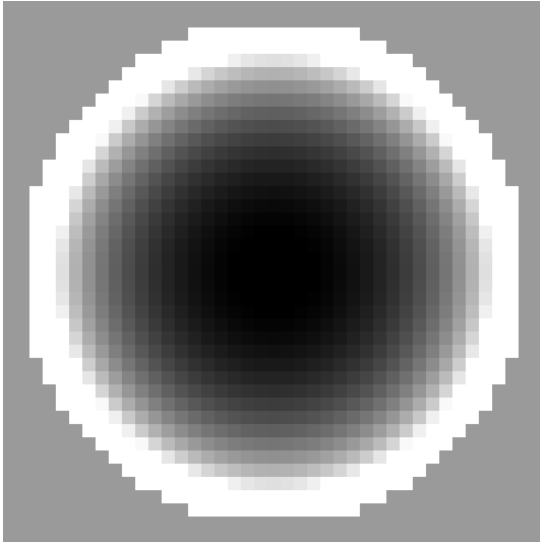


Figure 4. Pit template. White pixels are +1, black pixels are -1, and grey pixels in between. The medium grey pixels outside the white ring edge are exactly zero, thus not contributing to the convolution value. This particular pit template has a radius of 17 pixels, or 3.4 m.

#### 2.2.2.2.2 Merging of detections

In step 2, for each detection, if another detection is closer than the first detection's radius, the two detections are merged, keeping the stronger of the two detections. The distance between two detections is measured between their centres.

#### 2.2.2.2.3 Computation of attributes

In step 3, the following attributes are computed:

- Radius
- Correlation
- Normalized correlation value, that is, the correlation value divided by the radius.
- Average pit depth, measured as the height difference between the lowest point inside the pit and the average height on the ring edge outside the pit.
- Minimum pit depth, measured as the height difference between the lowest point inside the pit and the lowest point on the ring edge.
- Standard deviation of height values on the ring edge.

- Root mean square deviation from a perfect hemisphere, i.e., a perfect U-shaped pit.
- Root mean square deviation from a perfect V-shaped pit.
- For each pit, a threshold is defined as the value that separates the pixels inside the pit into two groups, the 25% of the pixels that are darker than the threshold, and the 75% that are brighter. Use this threshold to extract a dark segment from a square image centred on the pit, with sides equal to six times the radius. This is called the 25%-segment. If this results in a compact, central segment inside the pit, connected to a larger segment outside the pit, with only a few connecting pixels on a ring just outside the pit, then the central segment is separated from the outside segment. From the extracted segment, the following measurements are computed:
  - Offset: distance from pit centre to the segment's centre.
  - Major axis length, defined below in Section 2.2.2.2.4.
  - Elongation, defined as major axis divided by radius.
- Similarly to above, extract the 50%-segment and compute offset, major axis and elongation from that segment as well

#### 2.2.2.2.4 Major and minor axis, and elongation of a raster object

The major axis of an object can be computed from the central moments as (Prokop and Reeves, 1992):

$$\alpha = 2\sqrt{\frac{2(\mu_{20} + \mu_{02} + \sqrt{(\mu_{20} - \mu_{02})^2 + 4\mu_{11}^2})}{\mu_{00}}}$$

The minor axis is defined as

$$\beta = 2\sqrt{\frac{2(\mu_{20} + \mu_{02} - \sqrt{(\mu_{20} - \mu_{02})^2 + 4\mu_{11}^2})}{\mu_{00}}}$$

Here,  $\mu_{pq}$  is the central moment of order  $p+q$ :

$$\mu_{p,q} = \int_{-\infty}^{\infty} \int_{-\infty}^{\infty} (x - \bar{x})^p (y - \bar{y})^q f(x, y) dx dy ,$$

where  $f(x,y)$  is the object, and  $(\bar{x}, \bar{y})$  is the centre of gravity of the object. For the purpose of image axis computation, we are using a binary raster image representation of the object, with  $f(x,y)=1$  inside the object and  $f(x,y)=0$  elsewhere, so the central moments can be written as

$$\mu_{p,q} = \sum_{i=1}^N (x_i - \bar{x})^p (y_i - \bar{y})^q ,$$

where the summation is over the  $N$  object pixels. The centre of gravity is found from the regular moments  $m_{p,q}$ , and the general formulae are:

$$m_{p,q} = \int_{-\infty}^{\infty} \int_{-\infty}^{\infty} x^p y^q f(x, y) dx dy$$

$$\bar{x} = \frac{m_{1,0}}{m_{0,0}}$$

$$\bar{y} = \frac{m_{0,1}}{m_{0,0}}$$

Since we are using a binary raster image representation, this simplifies to

$$m_{p,q} = \sum_{i=1}^N x_i^p y_i^q$$

$$m_{0,0} = N$$

$$\bar{x} = \frac{m_{1,0}}{m_{0,0}} = \frac{1}{N} \sum_{i=1}^N x_i$$

$$\bar{y} = \frac{m_{0,1}}{m_{0,0}} = \frac{1}{N} \sum_{i=1}^N y_i$$

Having computed the major axis,  $\alpha$ , and the minor axis,  $\beta$ , the elongation can be computed. The elongation is usually defined as  $e=\alpha/\beta$ . However, for our purpose, we have a more stable measure of the minor axis in the form of the pit radius  $r$ . Ideally, we should scale the radius  $r$  by a constant  $c$  to get the elongation:  $e=\alpha/cr$ . However, for the 25% segment,  $e=\alpha/r$  is an acceptable estimate, although this elongation can be slightly less than 1 (Figure 5).

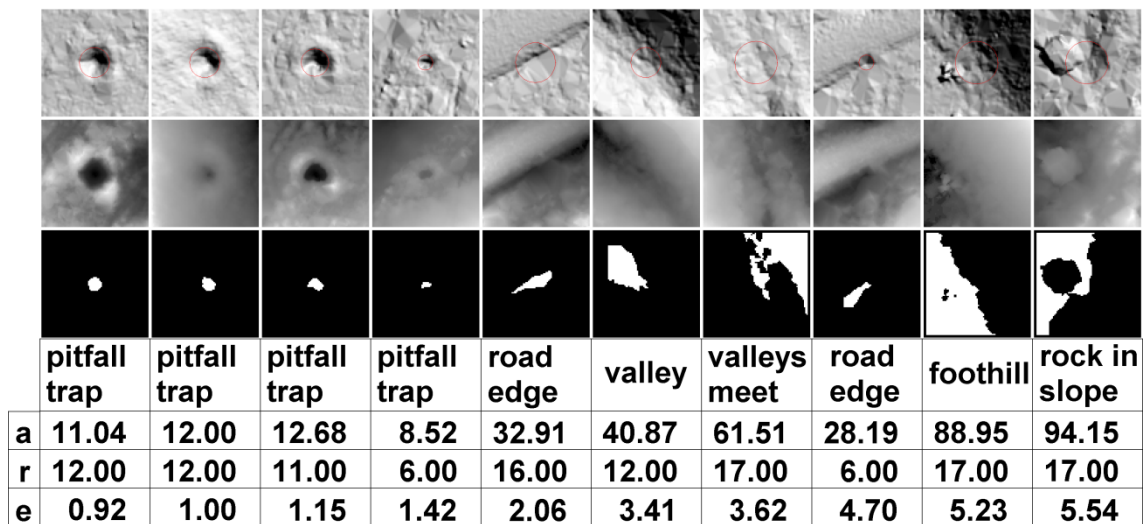


Figure 5. Elongation for four pitfall traps (left) and six false detections (right). Top row: hill-shaded DEM, second row: elevation image, with contrast adjusted for visualization, third row: 25% segments for detections, fourth to seventh rows: descriptions, major axes, radii, and elongations.

#### 2.2.2.2.5 Thresholds on measurement values

With true pits labelled, one can then sort the pit detections on one measurement at a time, to determine suitable thresholds that seem to be able to separate at least some false detections from the true detections. The thresholds should not be set too tight, as this may lead to true pits being removed by mistake in another dataset. In the event that one has a large number of training samples, one may use an attribute selection method (e.g., Somol *et al.*, 1999) and multivariate statistical analysis (e.g., Hastie *et al.*, 2009) to design a classifier.

We used the tile in Figure 3 as a guide in selecting a subset of the attributes and setting thresholds. Tight thresholds would have been

- normalized correlation > 4.5
- minimum depth > 0.4
- average depth > 0.75
- RMS u-shape < 0.075
- RMS v-shape < 0.075
- 25% segment elongation < 1.5

However, by setting the thresholds too tight, one may risk losing some true detections. Further, the datasets with reduced sampling density will probably need looser thresholds. So, we used:

- normalized correlation > 2.0
- minimum depth > 0.1
- average depth > 0.5

- RMS u-shape < 0.1
- RMS v-shape < 0.1
- 25% segment elongation < 4

We use this on the entire Olstappen dataset. All detections are manually checked by visual inspection of the hill-shaded lidar data. Each detection is labelled with a score 1-9, with 9 being an obviously correct detection, 5 being in doubt, and 1 being a clear misdetection. 2-3 mean probable misclassifications, but somehow resembling a pit. 4 is not used. 6-8 mean probable detections.

A selection of the automatic detections with manually assigned scores in the range 5-9 is checked in the field by archaeologists.

Next, the dataset is split in two parts: a training set and a test set, each containing half of the pits confirmed by archaeologists. The division was done by sorting the confirmed pits by the LAS file names in alphabetical order. We want the system to assign score values automatically to all detections. The score values should correspond to how confident the system is that a detection is a potential cultural heritage pit (Table 3). The automatic detections can then be overlaid on a map, with, e.g., separate colours for each confidence level, for subsequent field inspection.

Table 3. Confidence values and corresponding score values from the automatic method.

score value	confidence
1	very low
2	low
3	medium
4	medium high
5	high
6	very high

Table 4. Measurements for the pit detections.

attributes used in confidence estimation	attributes not used
normalised correlation	radius
minimum depth	correlation
average depth	standard deviation on edge
RMS difference from U-shape	50% blob offset
RMS difference from V-shape	50% blob major axis
25% blob offset	50% blob elongation
25% blob elongation	25% blob major axis

The training set contains 1129 automatic detections, of which 25 are confirmed pits by field inspection, 104 are pits confirmed by visual inspection only, and the remaining 1000 detections are regarded as non-pits by visual inspection only. Each of the 1129 detections have 14 attributes which may be used to assign confidence values (Table 4).

Table 5. Example thresholds for assigning confidence values to pitfall trap detections. For confidences 'very low' to 'high', all tests have to be fulfilled. \*However, a confidence of 'high' is upgraded to 'very high' if one or more of the tests in the 'very high' if one or more of the tests in the 'very high' column are met.

attribute	confidence					
	very low	low	medium	med. high	high	very high*
normalized correlation	≥1	≥2	≥2.5	≥3.0	≥3.5	
minimum depth	≥0.05	≥0.1	≥0.15	≥0.25	≥0.4	≥1
average depth	≥0.25	≥0.4	≥0.45	≥0.5	≥0.55	
RMS u-shape	≤0.2	≤0.1	≤0.09	≤0.08	≤0.07	≤0.02
RMS v-shape	≤0.2	≤0.1	≤0.08	≤0.07	≤0.05	≤0.015
25% blob offset	≤20	≤10	≤8	≤6	≤4	
25% blob elongation	≤4	≤2	≤1.75	≤1.5	≤1.25	
assigned tag	1	2	3	4	5	6

We sort the training set on each of the attributes in turn, to find reasonable thresholds for each of the confidence levels. Some of the attributes were found to have little discriminatory power, and thresholds were not used on these. This results in seven threshold tests (Table 5) in a combined IF-test. For a detection to get a specific confidence, say, 'medium', it has to fulfil all the seven threshold tests, that is:

```
IF (      (normalized_correlation >= 2.5) AND (minimum_depth >= 0.15)
      AND (average_depth >= 0.45) AND (RMS_u_shape <= 0.09)
      AND (RMS_v_shape <= 0.08) AND (25_percent_segment_offset <= 8)
      AND (25_percent_segment_elongation <= 1.75))
THEN confidence = 'medium'
```

The IF-tests are executed in the order of increasing confidence, from 'very low' to 'high'. For the confidence 'very high', the rule is different:

```
IF (      (confidence == 'high')
      AND (      (minimum_depth >= 1)
                OR (RMS_u_shape <= 0.02)
                OR (RMS_v_shape <= 0.015)))
THEN confidence = 'very high'
```

The detection obtains the best possible confidence according to these rules. Note that the thresholds in Table 4 and the above IF-tests are only example thresholds. The actual thresholds are optimized manually for the training set and are presented in Section 3.1.

### 2.2.2.3 Analysis of reduced point sampling density

In order to study the effect of reduced point density, the detection performance on the reduced versions are compared with the detection performance on the original version. All automatic detections in the full resolution are labelled as described above. Then, for each reduced sampling density, the automatic detections are compared with the automatic detections on the full resolution as follows. For each of the detections in the full resolution, the closest detection in the reduced resolution is located. If the distance between their centres is less than 2 m, then the detection is counted as 'found' in the reduced version.

## 2.3 Results

This section describes the experimental results. In Section 3.1, the results of using the method on the Olstappen data set from Nord-Fron municipality, Norway, are presented. Next, the results of the reduced point density experiments are given in Section 3.2. Then, experience from operational use in on-going field work in Øystre Slidre municipality, Norway, is described in Section 3.3.

### 2.3.1 Automatic detection of cultural heritage pits in lidar data of Olstappen

Before we could apply the automatic method on the test set, the thresholds for the confidence estimation step were optimized manually for the training set (Table 6). Of the 134 pits in the training set that were confirmed by archaeologists, 122 pits got 'medium' confidence or better (Table 7) by the automatic method, seven pits got 'low' confidence, and five pits were not detected. For the independent test set, the results were slightly worse, with fewer true detections with very high confidence, and more true detections with low or medium confidence than in the training set (Table 8). Still, the confidence levels reflect the number of true versus false detections in a meaningful way. All detections with 'very high' confidence are confirmed pits. Of the 'high' confidence detections, 2 of 28, or 7%, are false detections. Of the medium high confidence detections, 12 of 46, or 26%, are false. However, for the 'medium' and 'low' confidence detections, there are many more false detections than true detections. All in all, 5 of 134, or 4% of the pits confirmed by archaeologists were not detected by the automatic method. The five missing pits in the test set and the five missing pits in the training set were detected by manual visual inspection of a hill-shaded relief visualization the lidar data and included in the field inspection.

The confidence levels reflect the trade-off between detecting as many pits as possible, while at the same time limiting the number of false detection. E.g., 114 of 133 pits of archaeological interest were detected with medium confidence or better (Table 9); this is 85.7% of the pits of archaeological interest (Table 10). At the same time, 103 of the detections with medium confidence were false.

During the field work, an assessment was done for each pit to determine if it was a pitfall trap, a coal burning pit, or a flat coal burning site (Table 11). The majority of pits have not been surveyed in the field yet.

Table 6. Thresholds, optimized on the Olstappen training set, for assigning confidence values to pitfall trap detections. For confidences 'very low' to 'high', all tests have to be fulfilled. \*However, a confidence of 'high' is upgraded to 'very high' if one or more of the tests in the 'very high' column are met.

attribute	confidence					
	very low	low	medium	med. high	high	very high*
normalized correlation	≥2	≥2.5	≥2.5	≥3	≥3.5	
minimum depth	≥0.1	≥0.1	≥0.23	≥0.4	≥0.5	≥1.0
average depth	≥0.5	≥0.5	≥0.5	≥0.55	≥0.75	
RMS u-shape	≤0.2	≤0.1	≤0.07	≤0.05	≤0.04	≤0.02
RMS v-shape	≤0.2	≤0.085	≤0.07	≤0.05	≤0.03	≤0.015
25% blob offset	≤40	≤6	≤6	≤6	≤5	
25% blob elongation	≤4	≤2	≤1.5	≤1.3	≤1.2	
assigned tag	1	2	3	4	5	6

Table 7. The effect of running the automatic confidence assignment on the training set.

score value	1	2	3	4	5	6		
confidence	very low	low	medium	medium high	high	very high	not detected	sum
pit confirmed in field			2	2	5	16	1	26
modern/other visually								0
pit visually in image		7	27	32	17	21	4	108
not pit visually	329	517	136	15	3			1000
sum	329	524	165	49	25	37	5	1134

Table 8. The effect of running the automatic confidence assignment on the test set.

confidence	very low	low	medium	medium high	high	very high	not detected	sum
pit confirmed in field		3	21	17	12	8	6	67
pit visually in image	1	10	22	17	14	5		69
sum true pits	1	13	43	34	26	13	6	136
modern/other in field	1	1	1	1				4
not pit visually	384	375	90	11	2			862
sum	386	389	134	46	28	13	6	1002

Table 9. Accumulated counts for different confidence levels on the test set.

score value	≥1	≥2	≥3	≥4	≥5	≥6		
confidence	very low or better	low or better	medium or better	medium high or better	high or better	very high	not detected	sum
pit confirmed in field	61	61	58	37	20	8	6	67
pit visually in image	69	68	58	36	19	5		69
sum true pits	130	129	116	73	39	13	6	136
modern/other in field	4	3	2	1				4
not pit visually	862	478	103	13	2			862
sum	996	610	221	87	41	13	6	1002

Table 10. Classification rates.

score value	≥1	≥2	≥3	≥4	≥5	≥6
confidence	very low or better	low or better	medium or better	medium high or better	high or better	very high
pits detected	95,59 %	94,85 %	85,29 %	53,68 %	28,68 %	9,56 %
pits missed	4,41 %	5,15 %	14,71 %	46,32 %	71,32 %	90,44 %

Table 11. The various types of pit of archaeological interest in the two Olstappen data sets.

data set	Verified by field inspection				not verified	
	pitfall trap	pitfall trap, damaged	coal pit	flat coal-buring site	pit	uncertain pit
training set	21	0	0	13	108	3
test set	25	2	14	5	88	4
sum	46	2	14	18	196	7

The automatic detection method is able to locate pits of archaeological interest in varying surrounding landscape. Pitfall traps were detected in quite flat terrain (Figure 6a) and on a moderate ridge (Figure 6b). Also, a small pitfall trap that was overlooked during visual inspection of the lidar data, was detected by the automatic method (Figure 7).

However, there are also pits of archaeological interest that the automatic method fails to detect. At one location, two of four coal burning pits were missed by the automatic method (Figure 8). For the north-western of these (ID=290), the problem seems to be missing ground returns inside the pit due to trees (Figure 9). This makes the pit appear flat in the lidar height image. For the south-western of the four pits (ID=291), the pit is filled with tree branches. The north-eastern of the four pits (ID=187) is somewhat distorted in the lidar data, due to the trees on one side of the edge of the pit, but still the pit is detected by the automatic method with 'medium' confidence. The south-eastern of the four pits (ID=186) is quite small, with 2.5 m diameter, and not easy to spot in the field even on a short distance (Figure 9). Still, the pit is visible in the lidar data (Figure 8) and was also detected by the automatic method with 'medium' confidence.

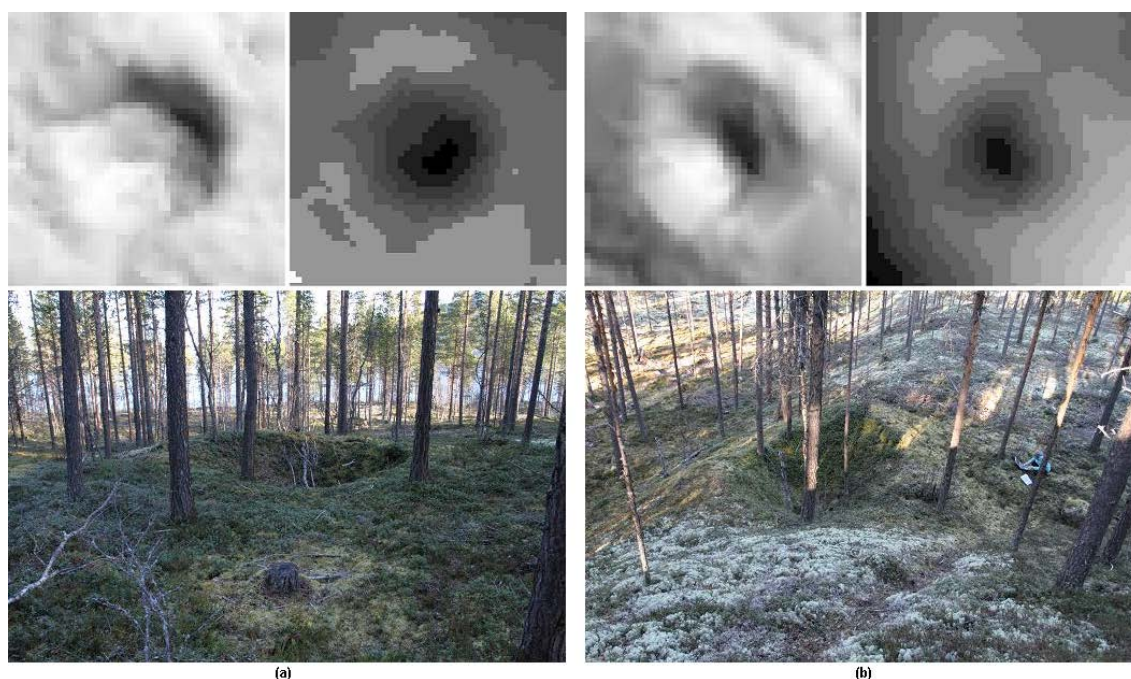


Figure 6. Two of the pitfall traps in the Olstappen training set. For each of the two pits, three images are given, in clockwise order: hill-shaded relief image, elevation image with 0.3 m resolution in height levels, and a field image. (a) A pitfall trap in a relatively flat terrain. (b) A pitfall trap on a moderate ridge.



Figure 7. A small pitfall trap in the Olstappen training set. This pit was not found during the initial visual inspection of the laser data, but detected by CultSearcher, and confirmed in the field. Upper left: hill-shaded relief image. Upper right: elevation image, 0.3 m height resolution. Bottom: field image.

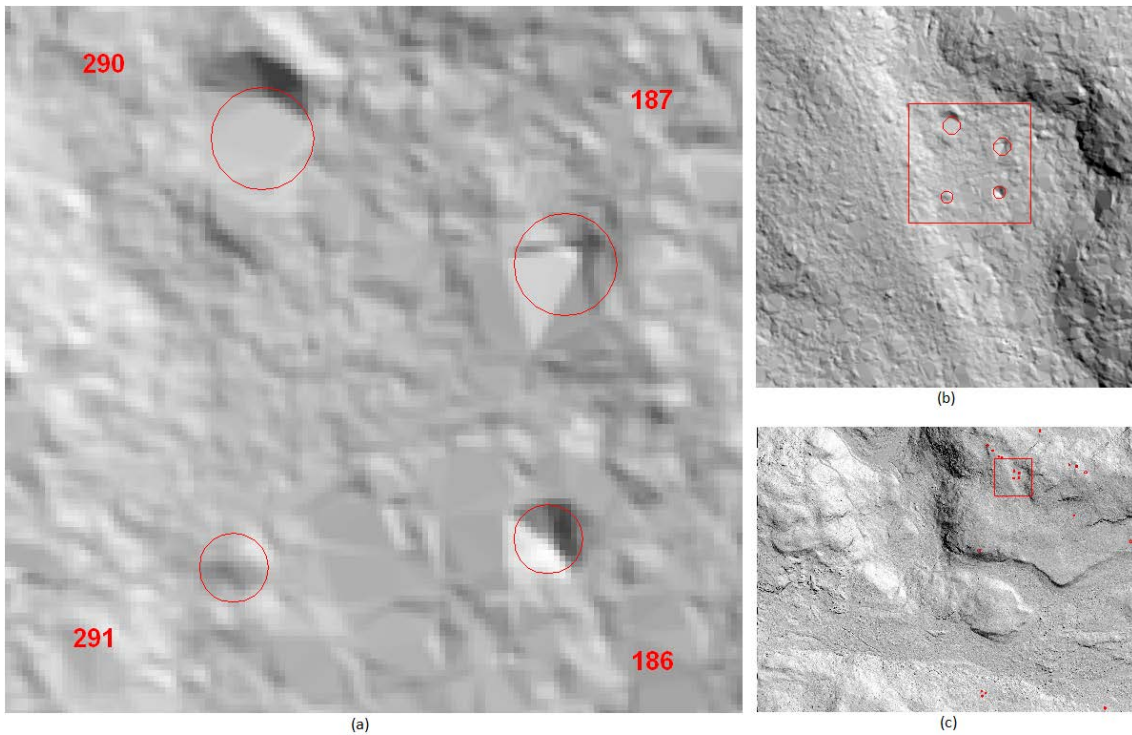


Figure 8. (a) A cluster of four coal pits at an iron extraction site in the Olstappen test set. The two leftmost pits were not detected by the automatic method, but detected visually and confirmed in the field. The two other pits were detected by the automatic method, with medium confidence. The image in (a) is the area covered by the red square in (b), and the image in (b) is the area covered by the red square in (c). The entire image in (c) is a 600 m by 800 m tile.



Figure 9. Photos from field inspection of the iron extraction site in Figure 8.

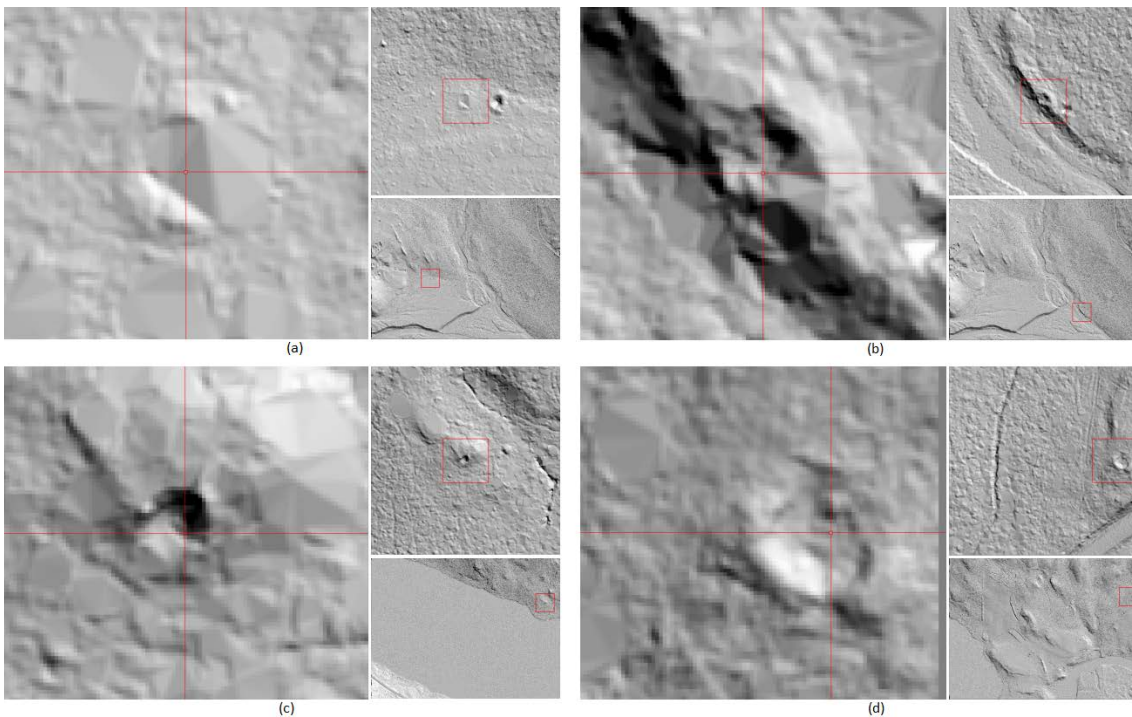


Figure 10. Examples of pits in the Olstappen training set that were not detected by the automatic method, but detected visually in the lidar data. (a) The pit (ID=14) appears very flat, there seems to be missing ground returns in the data, probably due to trees. (b) A pit (ID=19) located on a narrow ridge with a steep cliff on one side. (c) Pit (ID=271) with irregular shape. (d) Pit (ID=276) with irregular shape.

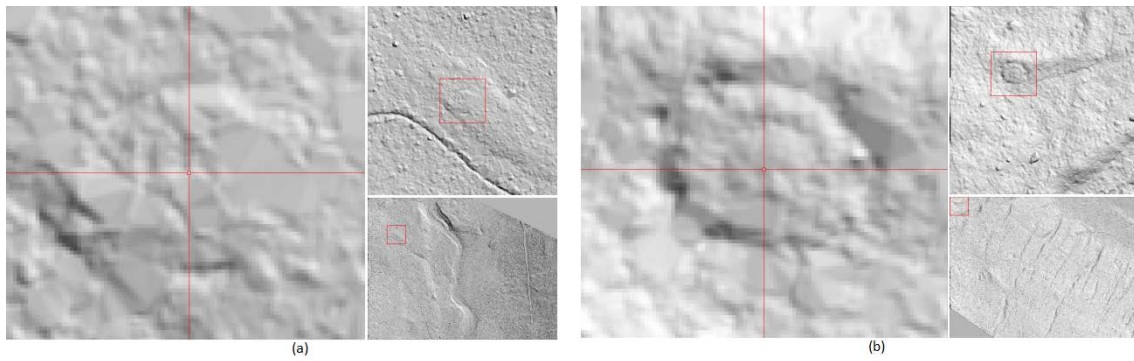


Figure 11. Examples of flat coal burning sites that were not detected by the automatic method, but detected visually in the lidar data. (a) ID=31, (b) ID=62.

The problem with missing ground hits inside pits due to trees is also observed at another location (Figure 10a). On one occasion, the automatic method did not detect a pit located on a narrow ridge with a steep cliff on one side (Figure 10b). Also, the automatic method did not detect pits with shapes that deviated too much from ideal pits (Figure 10c-d).

During the field work, 16 charcoal burning sites were found (Figure 11-Figure 13). Each charcoal burning site is often surrounded by a circular, shallow ditch, but is otherwise flat (Figure 11) or heap-shaped (Figure 12-Figure 13). Except for one, these were not detected by the automatic method. Since the automatic method is not designed to detect such shapes, the missed charcoal burning sites are not counted in Table 7-Table 9.

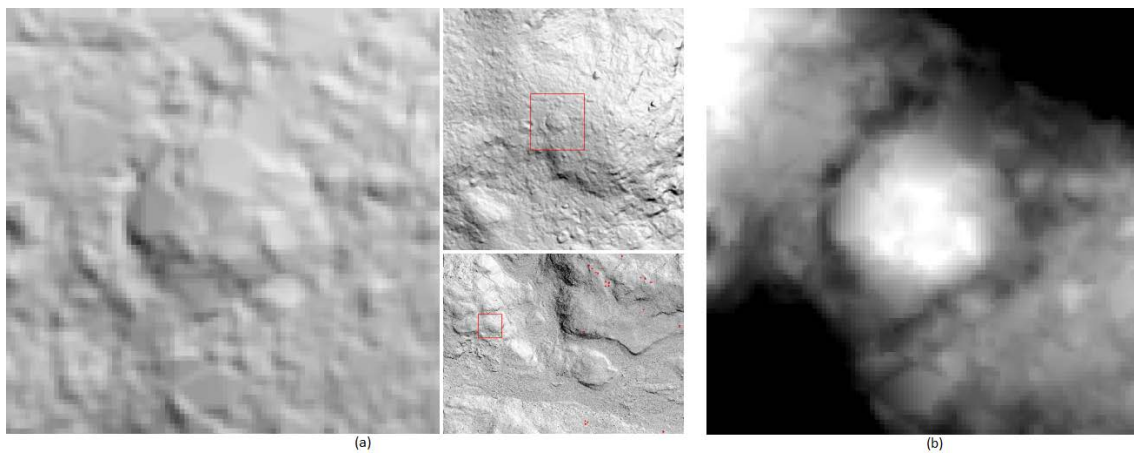


Figure 12. A heap-shaped coal burning site (ID=155). (a) Hill shaded relief image, at different zoom levels. (b) Elevation image, with bright areas having a higher elevation than dark areas. The heap is 0.4 m high and is surrounded by a shallow ditch.



Figure 13. Photo from field inspection of the heap-shaped coal burning site (ID=155) in Figure 12.

Another potential problem with the automatic method is pits that are split on a tile boundary, or are so close to the edge that the pit templates, which are centred on the pit, would be partially outside the image. We have only seen one example of this in the Olstappen dataset (Figure 14).

On the other hand, the automatic method was able to detect two partially collapsed pitfall traps, but with low confidence (Figure 15).

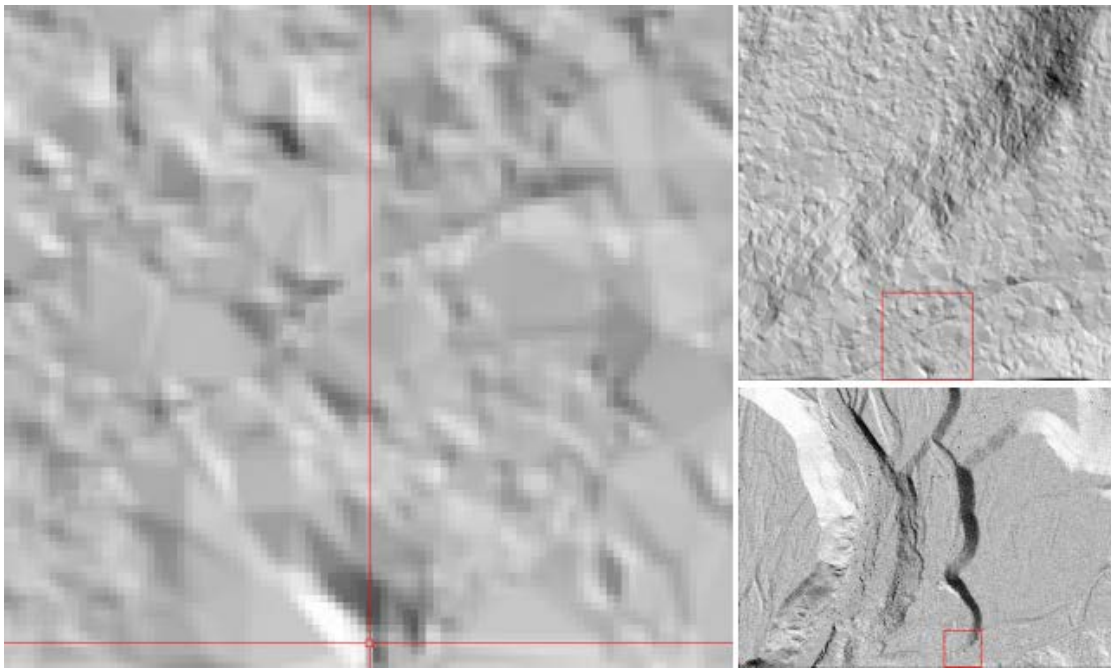


Figure 14. A pit located close to the tile edge. This pit was not detected by the automatic method.

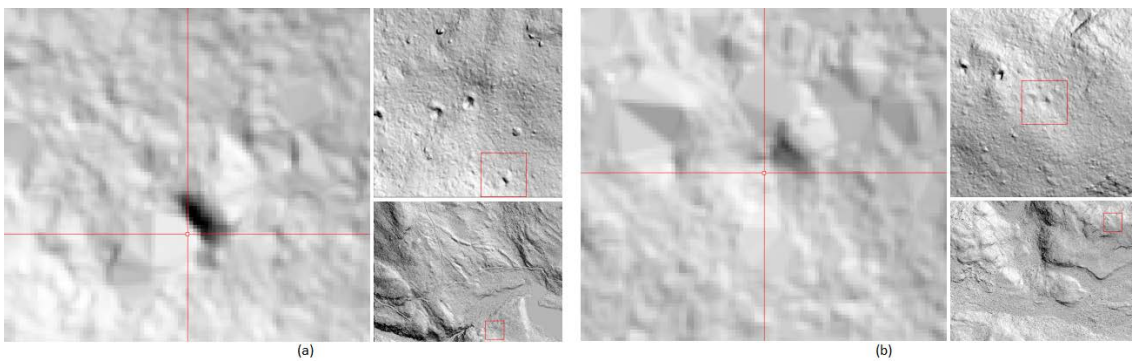


Figure 15. Partly collapsed pitfall traps in the Olstappen test set. These pits were detected by the automatic method with 'low' confidence.

### 2.3.2 Detection of pits in reduced versions of lidar data

The analysis described in Section 2.2.3 was performed on the entire Olstappen dataset (Table 12).

For the purpose of measuring the reduced detection on the datasets with reduced point density, one may consider detections of categories 5-9, spanning the detections labelled 'in doubt', 'probable detection' and 'certain detection'. These are 262 in total. For the datasets of reduced point densities, the number of detections is given in the two rightmost columns of Table 12 as absolute and relative figures.

By inspecting the reduced point density datasets, it can be observed that all pits are degraded in shape as the point density is reduced (Figure 16), but that small pits are more affected than large pits. E.g., at 0.29 ground returns per m<sup>2</sup>, the two larger pits are still detected and still resemble pits (Figure 16), one pit has completely vanished, and one other small pit is so degraded that it is difficult to see.

Table 12. Detection results on reduced point density datasets. Detection categories are from a manual inspection of the detection results on the full resolution dataset, with '9' being a certain true detection of a cultural heritage pit, '5' being in doubt, and '1' being a certain false detection. Categories 2-3 are probable false detections, with something resembling a pit. Categories 6-8 are probable cultural heritage pits.

point density		manually assigned score 1-9										
factor	per m <sup>2</sup>	1	2	3	4	5	6	7	8	9	Sum 5-9	
1	7,277	1756	164	42	0	35	6	59	53	109	262	100,00 %
0,9	6,549	1458	141	40	0	33	5	58	53	109	258	98,47 %
0,8	5,822	1295	136	33	0	32	5	56	52	107	252	96,18 %
0,7	5,094	1170	124	32	0	30	6	56	52	107	251	95,80 %
0,6	4,366	1065	108	28	0	29	4	52	53	107	245	93,51 %
0,5	3,638	947	97	28	0	26	4	49	52	106	237	90,46 %
0,4	2,911	806	79	24	0	21	4	49	50	103	227	86,64 %
0,3	2,183	636	75	17	0	19	4	46	46	103	218	83,21 %
0,25	1,819	559	62	18	0	17	4	44	44	105	214	81,68 %
0,2	1,455	482	53	13	0	15	3	37	42	101	198	75,57 %
0,15	1,092	360	43	16	0	11	2	31	41	91	176	67,18 %
0,1	0,728	252	33	9	0	6	2	23	34	82	147	56,11 %
0,08	0,582	198	29	9	0	6	0	21	29	74	130	49,62 %
0,06	0,437	143	22	6	0	6	0	14	21	71	112	42,75 %
0,04	0,291	94	16	3	0	3	0	9	12	47	71	27,10 %
0,02	0,146	35	4	0	0	1	0	1	3	26	31	11,83 %
0,01	0,073	15	1	0	0	2	0	0	3	9	14	5,34 %
0,005	0,036	6	0	0	0	0	0	0	0	1	1	0,38 %
0,003	0,022	2	0	0	0	0	0	0	0	0	0	0,00 %
0,001	0,007	0	0	0	0	0	0	0	0	0	0	0,00 %

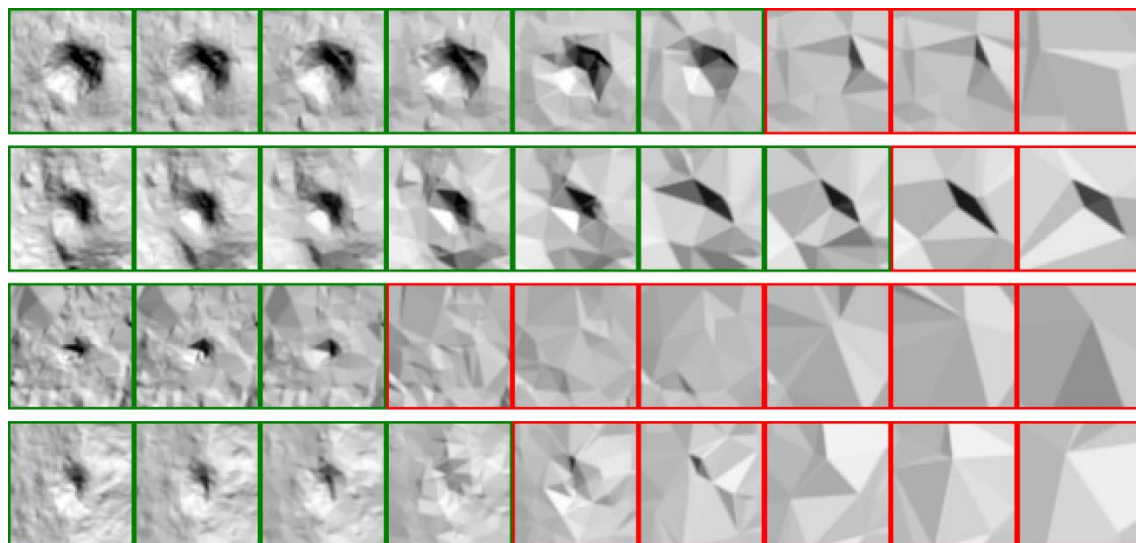


Figure 16. Four pitfall traps at nine different point densities. From left to right: original dataset with 7.3 ground points per m<sup>2</sup>, reduced dataset with 3.6 points per m<sup>2</sup>, 1.8 points per m<sup>2</sup>, 0.73, 0.29, 0.15, 0.073, 0.036, and 0.007 points per m<sup>2</sup>. A green frame indicates that the pitfall trap is detected at this resolution, while a red frame indicates that it is not detected.

By plotting the detection percentages, relative to the full resolution dataset, as a function of point density per m<sup>2</sup> (Figure 17), the recognition rate drops slowly from 100% to 82% as the point density is reduced from 7.3 to 1.8 ground points per m<sup>2</sup>. When the point density is reduced further below 1.8 points per m<sup>2</sup>, the recognition rate drops more rapidly, reaching 50% at around 0.6 ground points per m<sup>2</sup>.

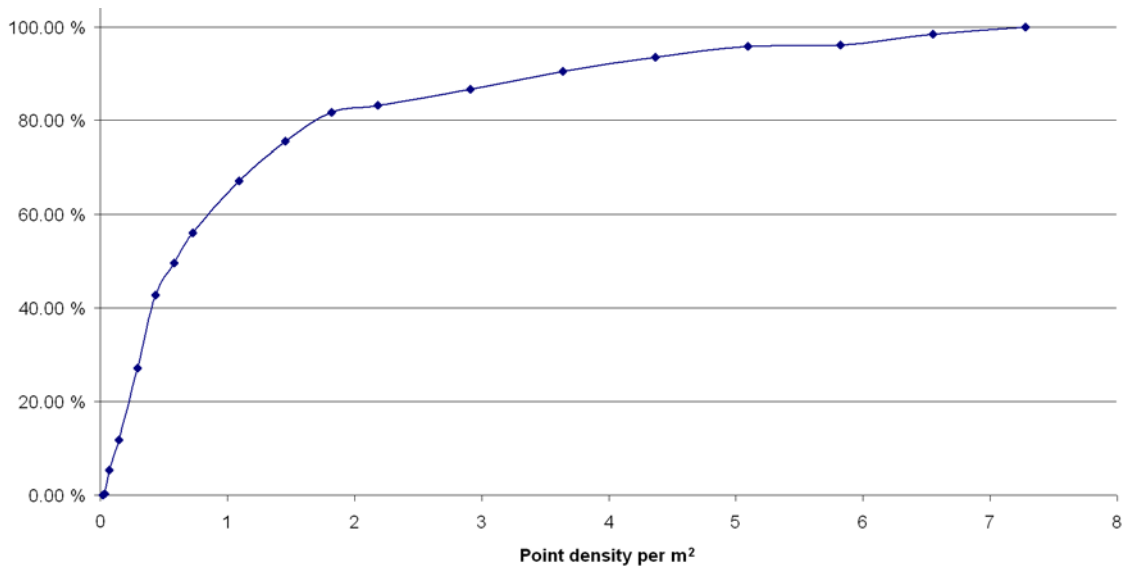


Figure 17. Detection rates as a function of point density, relative to the full resolution dataset.

Based on this analysis, it was decided to acquire the lidar data for Øystre Slidre municipality with 5 emitted laser pulses per m<sup>2</sup>.

### 2.3.3 Operational use in Øystre Slidre municipality, Norway

Øystre Slidre municipality is known to contain many ancient iron production sites, with charcoal burning pits as the most prominent visual appearance today. These are, in general, more varying in size than the pitfall traps which dominated the Olstappen data set. Further, it was considered more important to assign medium confidence or better to most of the true pits than to limit the number of false detections with medium confidence or better. In most cases, the false detections can be recognized as unlikely from the context of the landscape by an archaeologist. Therefore, we used lower thresholds (Table 13) in the method that assigns confidence values to the detected pits.

Table 13. Adjusted thresholds for the Øystre Slidre dataset.

feature	confidence					
	very low	low	medium	med. high	high	very high*
normalized correlation	≥1	≥2	≥2,5	≥2,5	≥2,5	
minimum depth	≥0,05	≥0,1	≥0,15	≥0,25	≥0,4	≥1
average depth	≥0,25	≥0,4	≥0,45	≥0,5	≥0,55	
RMS u-shape	≤0,2	≤0,1	≤0,09	≤0,08	≤0,07	≤0,02
RMS v-shape	≤0,2	≤0,1	≤0,08	≤0,07	≤0,06	≤0,015
25% blob offset	≤20	≤10	≤10	≤10	≤10	
25% blob elongation	≤4	≤2	≤1,75	≤1,5	≤1,5	
assigned tag	1	2	3	4	5	6

The goal of the on-going large-area survey in Øystre Slidre is to secure a trustworthy basis for heritage management in an area with few registered ancient monuments, but a large unregistered number of such monuments. After laser scanning the data was submitted to the heritage management authorities for visual inspection and to the Norwegian Computing Center for automatic detection. The resulting inspection and detection files were then submitted to the

field crew. Control of objects in the field was undertaken using a Leica DPOS for guidance, which displays both visually inspected and automatically detected objects on a projected map. This procedure is extremely efficient and cuts field time by about 90 %, compared to traditional surface surveys.

After the automatic detection method had been applied, false detections along roads and water courses were manually assigned very low confidence for 36 tiles. However, in the subsequent field work, it was found that this was not so important, as these situations were easy to spot in the relief shaded printouts of the lidar data that were used in the field work. So, the manual re-assignment of confidence for detections along roads and water courses was dropped for the remaining tiles.

Initially, most emphasis was placed on the visually found objects, while automatically detected pits were checked if they had 'high' confidence or if they were situated in groups, typically for iron extraction sites. Quickly, however, the field crew discovered that in many instances even 'low' confidence objects were ancient pits. Following this discovery most automatically detected objects were checked in the field – if not obviously false. This led to the discovery of a number of sites, unnoticed by visual inspection of the data.

As an example of a typical field day, a GPS track was recorded at Yddin in Øystre Slidre municipality (Figure 18). The track measures 5.8 km (3.6 miles) and was accomplished within four hours. The track visited 47 automatic detections and an additional ten visual detections, all marked on the map prior to the field work. The resulting map of archaeological interpretations gave 13 iron extraction sites and four single charcoal burning pits (Figure 19). One of the iron production sites was not detected visually in the lidar data (Figure 20).

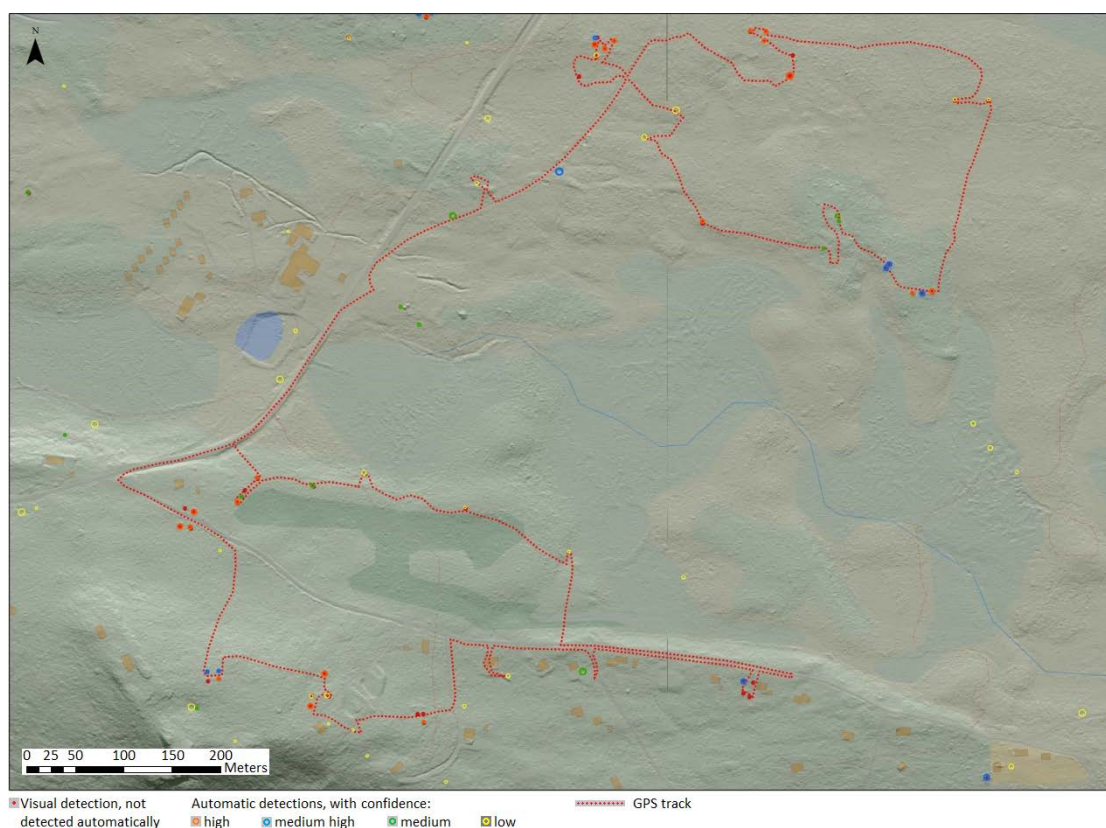


Figure 18. GPS track of field work at Yddin, Øystre Slidre municipality, Oppland County, Norway.

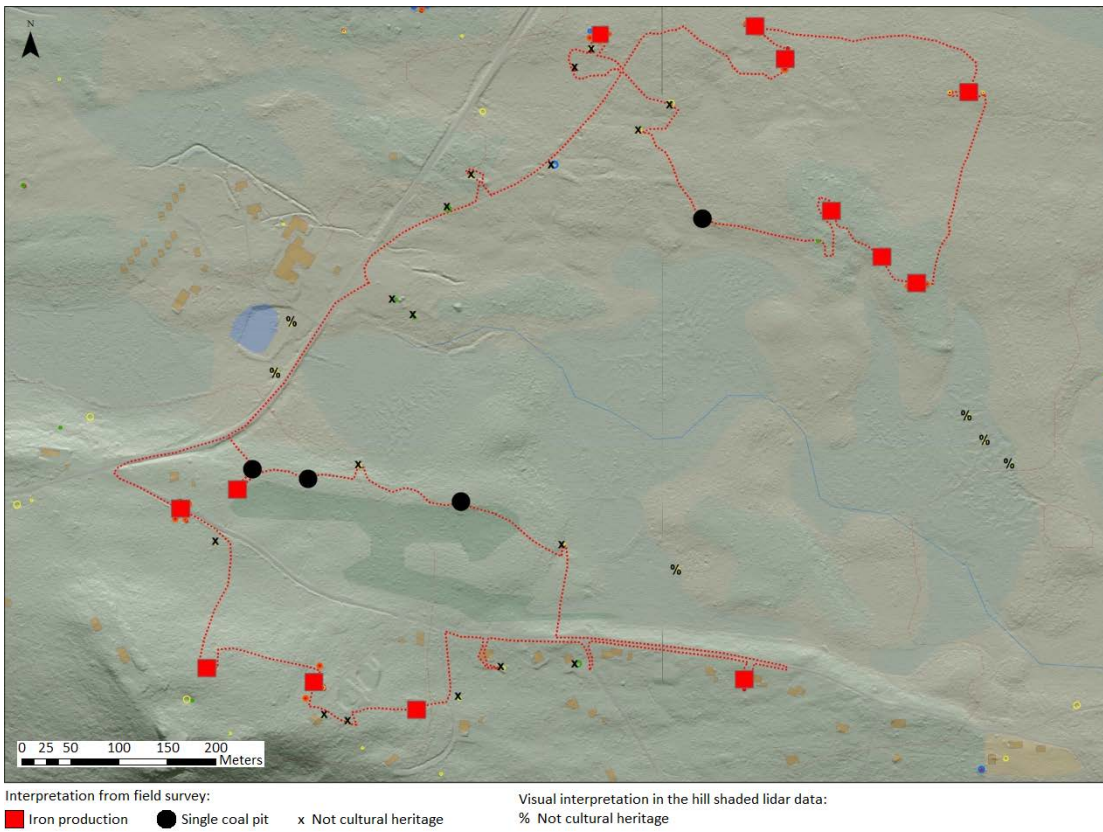


Figure 19. Archaeological interpretation of detected pits at Yddin.

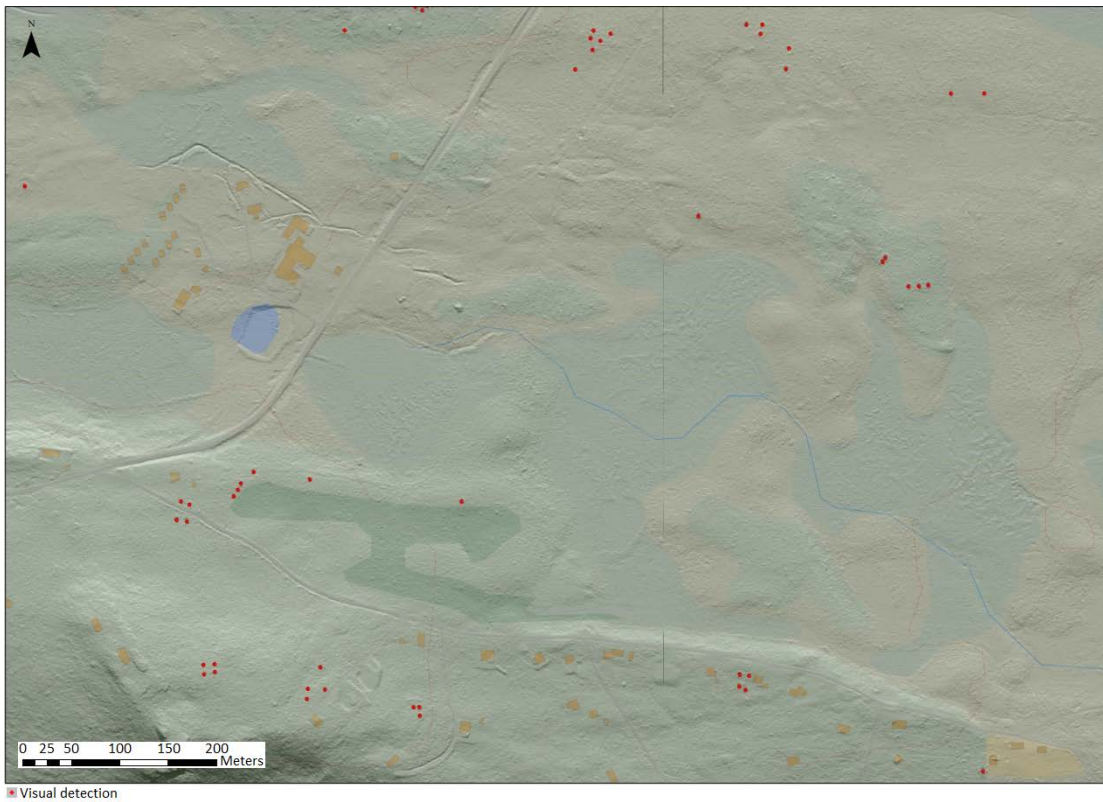


Figure 20. Visual detections at Yddin.

Some areas contained a very high number of detections, so high that suspicion arose beforehand that natural characteristics of the terrain were the cause. This was confirmed by field inspection. In such areas only objects with 'high' confidence were checked initially, and only if these objects proved to be 'true' did field confirmation extend to object of 'low' confidence.

Experience from the field work suggests that automatic detection is clearly superior to visual inspection of the lidar data in finding small pits or pits that are not easily visible. Visual inspection is better at finding additional information on sites, because human interpretation based on archaeological knowledge can be applied. Combining these two methods secures a very good basis for the subsequent field survey. Also, automatic detection replaces the need for tedious, accurate manual digitizing of pit locations, leaving the operator to accept pits in a yes/no manner. Only the few missed pits need to be accurately digitized manually.

## 2.4 Discussion

The detection results on the Olstappen test set indicate that the automatic method is capable of detecting 95% of the pits of archaeological interest that were visible in the terrain, while at the same time getting four times as many false detections as true detections. Experience from field work indicates that this is an acceptable trade-off. Further, it was observed that the automatic method was able to detect several small pits that were overlooked by visual inspection of the lidar data. The combined use of automatic detection and visual inspection prior to field survey is now being used by archaeologists in Oppland County, Norway, for the mapping of ancient hunting systems and iron production sites.

Since the automatic method was trained on one geographic area and tested on an adjacent geographic area, one could risk that the method was optimized for this area only, and not necessarily applicable in other geographic areas, with other varieties of pits of archaeological interest. To compensate for this, the confidence thresholds were slightly relaxed before the automatic method was applied to the Øystre Slidre dataset. The on-going field survey in Øystre Slidre municipality indicates that the automatic method is able to capture almost all pits of archaeological interest in this area as well, and that many of the false detections can be spotted quite easily by an experienced archaeologist.

The automatic method is not designed to detect flat or heap-shaped charcoal burning sites. It would have been useful if the automatic method were able to detect these as well. However, one major obstacle is the low number of training samples of such sites. Also, they are less visible in the data, and, therefore, more difficult to detect by an automatic method. Another possible extension could be to detect intact grave mounds, which are heaps of roughly the same size as the pitfall traps. There are forested areas in Vestfold County, Norway, that are known to contain intact grave mounds, and when lidar data of sufficient point density of such areas become available, one can attempt to extend the method to detect grave mounds and, possibly, other heaps of archaeological interest. Further, there is a need for an automatic method to detect linear structures in lidar data, such as stone fences and walls.

The results of the experiments with reducing the point density of lidar data indicate that 1.8 ground returns per m<sup>2</sup> is a minimum requirement for the detection of pitfall traps. It should be stressed that the point densities in the experiments are ground returns, excluding vegetation and building returns. The specifications of the datasets refer to the number of emitted pulses, some of which never reach the ground. Therefore, when the experiments suggest that at least 1.8 ground hits per m<sup>2</sup> is needed, this means that the total number of emitted pulses per m<sup>2</sup> may

need to be higher. How much higher depends on the vegetation density: denser vegetation needs a higher number of emitted pulses to maintain the same ground return density. For our data sets, about 70% of the emitted laser pulses hit the ground, requiring about 2.5 emitted pulses per m<sup>2</sup> as a minimum. Further, increased point density makes visual interpretation easier, which is important if one wishes to visually verify automatic detections and identify false detections and missing detections. Also, if smaller archaeological features are to be mapped, higher point density is needed. As a general advice, one should acquire lidar data at a very high density for an initial, representative small part of area to be mapped. Then, a point reduction experiment can be conducted to determine the required point density.

The Norwegian Mapping Authority has started a national lidar data acquisition in order to produce a new national digital elevation model, with an acquisition resolution of 0.7 emitted pulses per square meter. For the Olstappen dataset, this would result in about 50-55% recognition rate.

Three other effects are not addressed in the point reduction experiment. First, the flying height is higher when acquiring lower point densities, meaning that the footprint on the ground of each emitted laser pulse is larger, which means that the measured elevation is averaged over a larger area. Second, the shape of the pitfall traps and other pits are more distorted (Figure 15), meaning that the manual inspection of the detection results could be more difficult. In the present experiment, one had the luxury of doing the manual inspection on the full resolution dataset. Third, the number of false detections may increase.

In the point reduction experiment, a detection can be moved by up to two meters and still be valid. We have not investigated how much the detections actually moved in the reduced datasets. Obviously, if detections are moved, this has implications on the accuracy of the centre coordinates of pits. Similarly, reduced point density has implications on the measured radii and depths of pits.

In the Olstappen dataset, we observed that a large number of false detections occur at water courses and along roads (e.g., footpath tunnels, bridges over small creeks, etc.). To remove these, GIS layers for roads and water courses could be used to mask these areas. The reason that these false detections occur at all is that we have to tolerate quite substantial deviations from an ideal pit to capture the true archaeological pits. The amount of deviation is reflected in the confidence levels.

When generating the DEM, we used the lidar returns that were labelled 'ground' by the lidar data provider. During field survey, we have observed that low vegetation is sometimes confused with the ground, which occasionally may lead to false pits in the DEM. Coluzzi et al (2010) used full waveform lidar to better discriminate between ground and low vegetation. At the moment, full waveform lidar data is not collected by the commercial lidar data providers. However, this is likely to change in the future, as also the forest industry is interested in full waveform lidar for better forest inventory estimation (e.g., see Pirotti, 2011).

It should be stressed that no automatic method can be expected to find 100% of the phenomena of archaeological interest in a dataset. Further, no single dataset can be expected to produce a complete archaeological map. Even a combination of different data sets, be it lidar data, aerial an satellite images, hyper-spectral scanning, and/or geophysical survey, must be expected to give an incomplete archaeological map (Powlesland, 2011). Indeed, the absence of evidence must not be taken as an evidence of absence of archaeology (Powlesland, 2011). Having said all

this, automatic methods may be an important tool in providing more complete and accurate archaeological maps, especially when applied on lidar data with a large number of phenomena of archaeological interest.

In conclusion, we have demonstrated that semi-automatic detection of hunting systems and iron extraction sites in lidar data is a valuable tool in combination with visual inspection of the lidar data, prior to subsequent field survey. Provided that the point density of the lidar data is high enough, the field survey can be accomplished ten times faster compared to the traditional approach without lidar data. Obviously, this is mainly due to the use of lidar data in itself, but automatic detection contributes both by reducing the time required for visual interpretation and by detecting pits that are missed during visual inspection.

### 3 Automatic detection of grave mounds in lidar data

In 2011, some initial experiments were conducted, with the aim of determining whether it would be possible to adapt the automatic detection method to identify heaps in the lidar data. These heaps could be ancient grave mounds. For this purpose, we have obtained lidar data from Larvik municipality in Vestfold County.

We are using the same measurements of deviation from an ideal shape as for pits, and the initial experiments suggests that

1. Most heaps can be detected
2. The heaps are, in general, less distinct than the pits
3. More false detections are being made compared with automatic detection of pits
4. The range of sizes suggests a multi-resolution approach.

Below are some examples of heap detections in Larvik municipality, Vestfold (Figure 21-Figure 24).

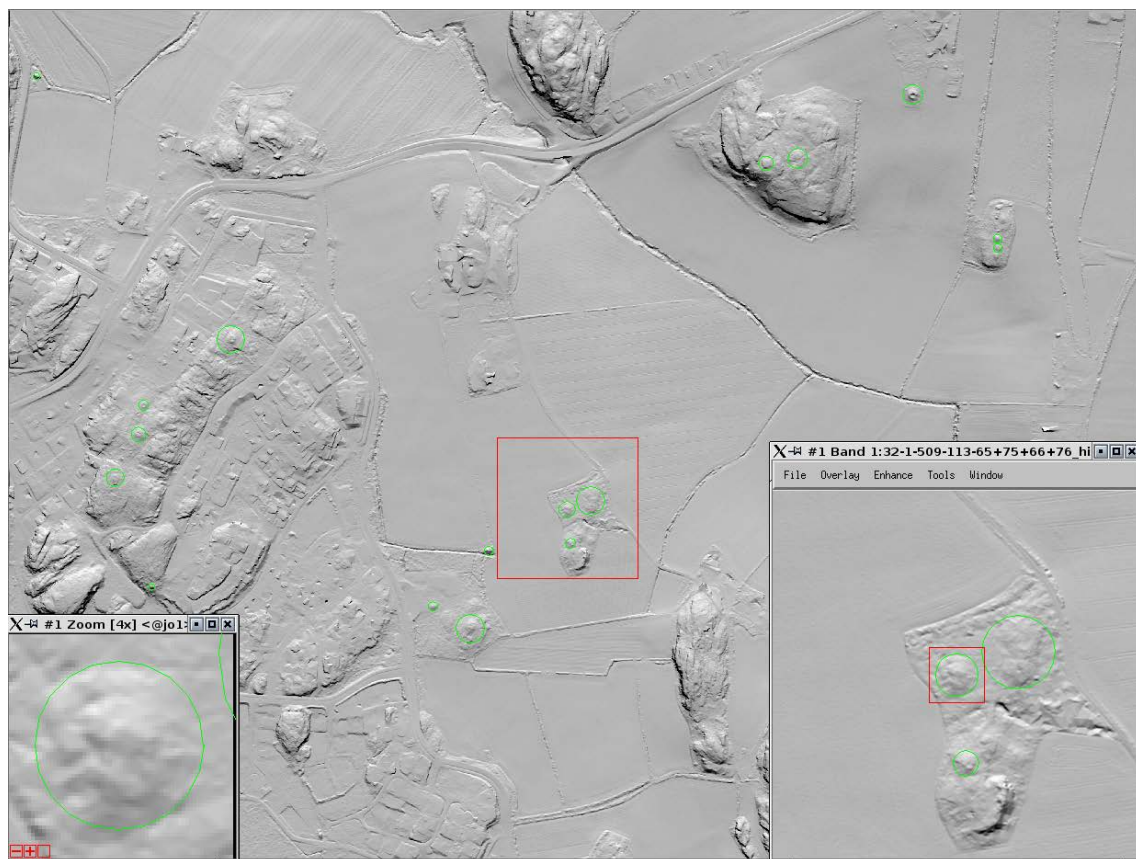


Figure 21. Automatic detections at Valby, Larvik municipality, Vestfold. The highlighted area in the overview image contains four known grave mounds in a forested area, enlarged in the lower right part of the figure. The single grave mound further enlarged in the lower left part of the figure was photographed during fieldwork (Figure 22).



Figure 22. One of the grave mounds in the small forest patch south of Valby, Larvik municipality, Vestfold County.

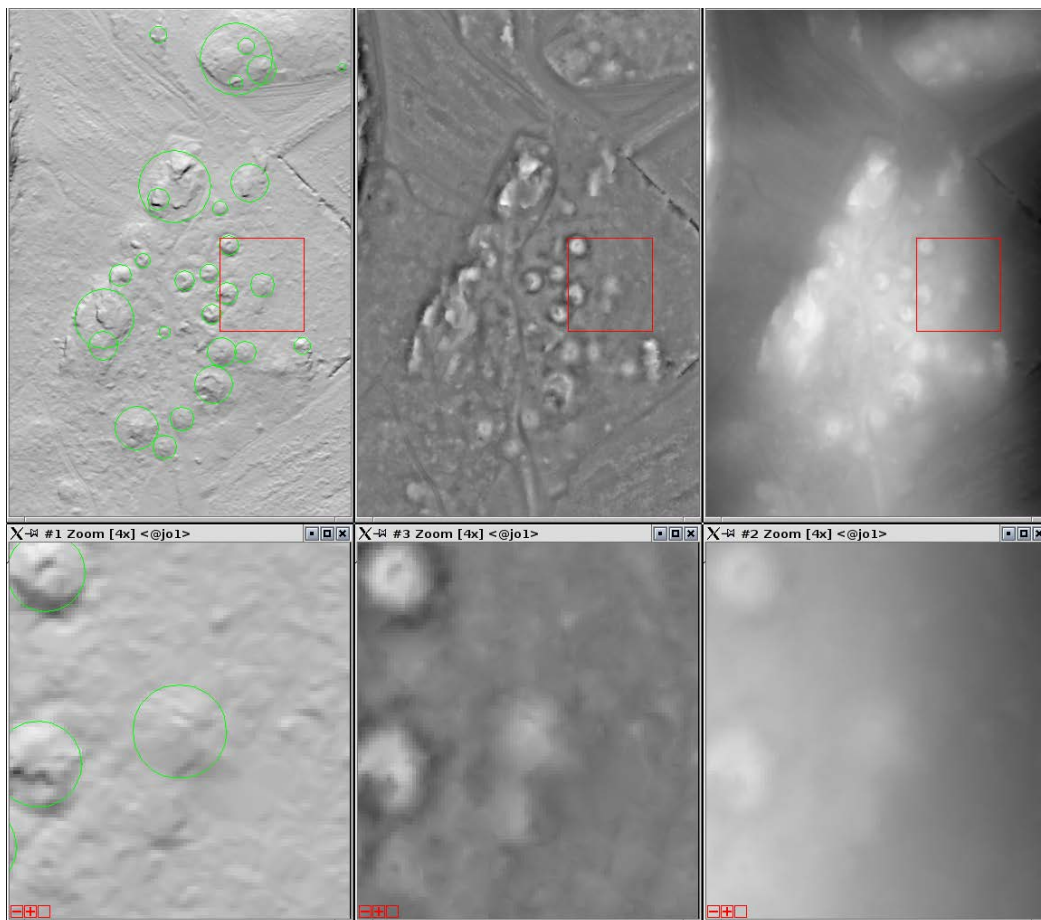


Figure 23. Preliminary results of heap detection in lidar data from Larvik municipality. Left: Hillshaded relief, with detections in elevation image superimposed. Middle: Local height image. Right: elevation image.

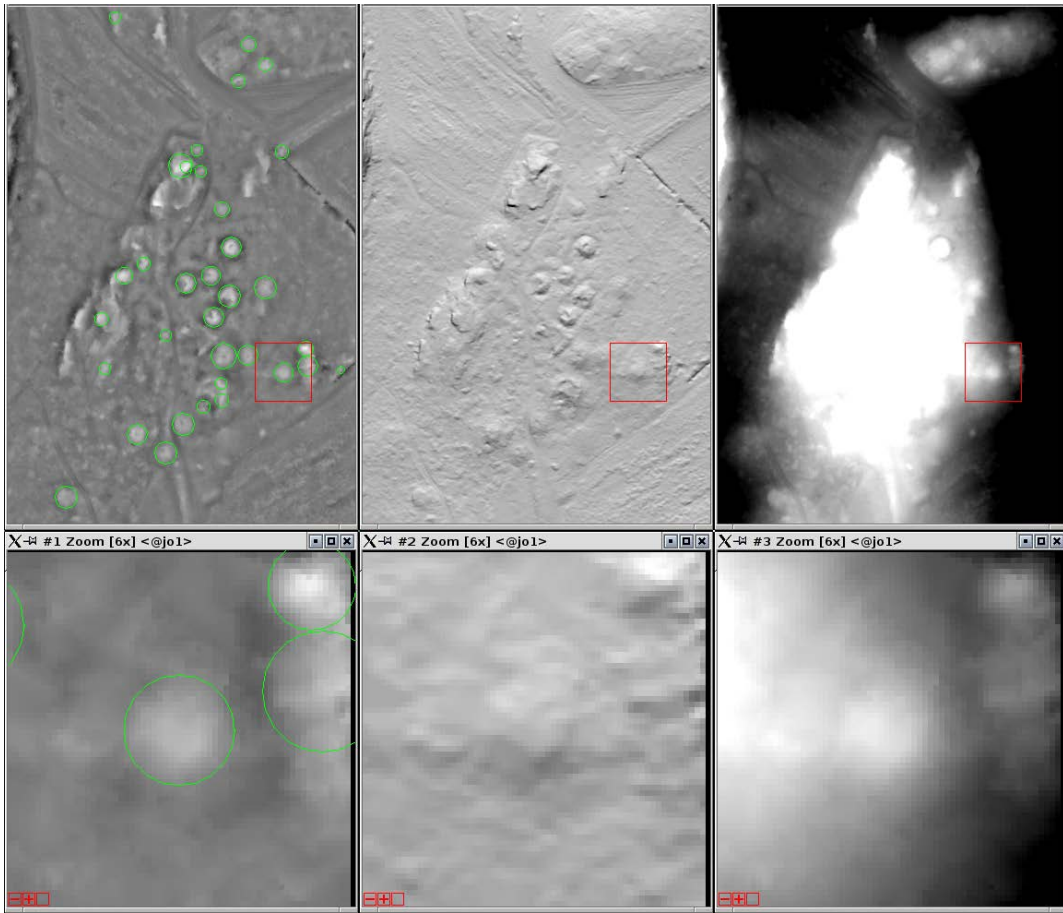


Figure 24. Detection result on a local elevation model, where the average height in a region surrounding each pixel has been subtracted from the measured height value. Thus, emphasis is placed on the local height variations.

## 4 Acquisition of satellite imagery

Inspired by the crop mark detections made on satellite images from 2009 and 2010, we acquired repeated Worldview-2 images for Tjølling and Brunlanes during the summer of 2011 (Table 14). However, despite collecting six repeated acquisitions for each area, no clear crop mark detections were made. This is most likely due to a very wet summer in southern Norway in 2011. We plan to continue acquiring Worldview-2 images in 2012, but the budget will probably limit the total number of acquisitions to about four.

Table 14. Worldview-2 acquisitions during 2011. All images were ordered as 8-band multispectral 2.0m resolution) plus panchromatic (0.5 m resolution).

	Brunlanes	Tjølling
11 July 2011	x	x
27 July 2011	x	x
2 August 2011	x	x
23 August 2011	x	x
1 September 2011	x	x
9 September 2011	x	x

For most 2010 detections in the Tjølling (7 August 2010) and Brunlanes (16 July and 7 August 2010) images, there were no clearly visually apparent crop marks in the 2011 images (e.g., see Figure 25). However, there were a few exceptions. For the crop mark at Huseby (Figure 26), there is a dark spot in the 1 September 2011 image. For a crop mark at 561140E, 6551309N, there is another circular crop mark to the south in the 1 September 2011 image (Figure 27).

For a crop mark at 557901E, 6538291N in the 7 August 2011 Brunlanes image, there are traces of circular structures in some of the 2011 images (Figure 28). For another crop mark at 556411E, 6540068N, there are crop marks in several of the 2011 images (Figure 29).

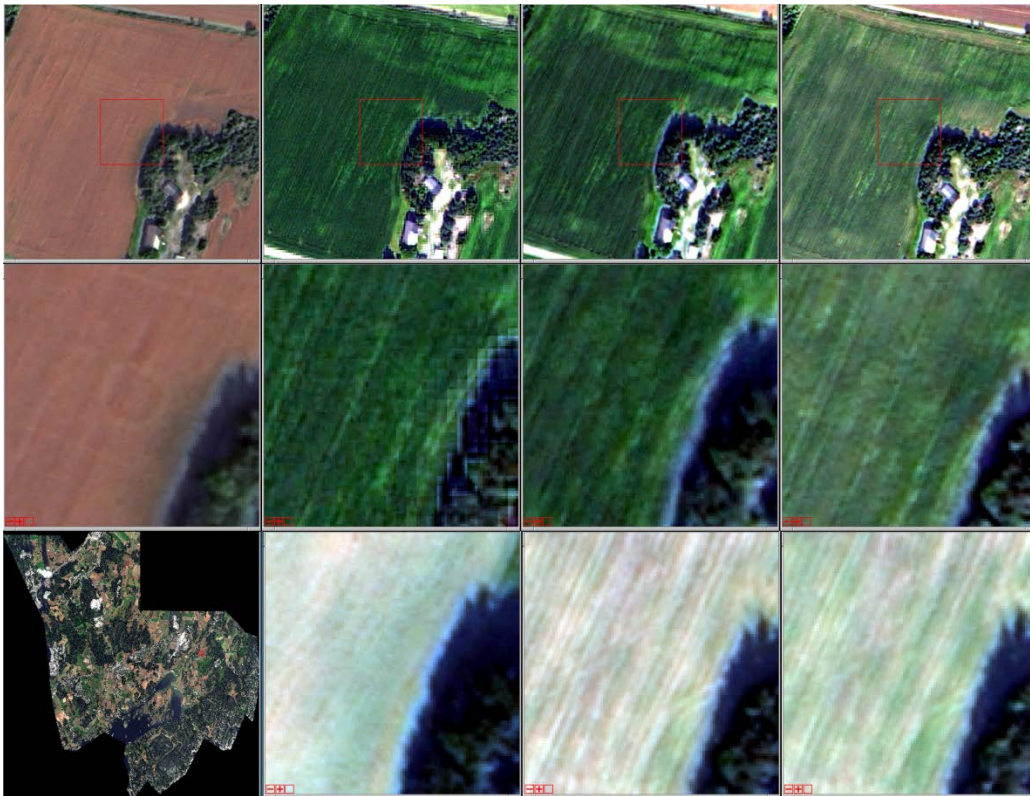


Figure 25. Time series of Worldview-2 images of crop mark at Eide. Top row, from the left: (1) crop mark at Eide in image of 7 August 2010. (2-4) Same area in images of 11 July 2011, 27 July 2011, and 2 August 2011. Middle row: Detail of top row, the parts inside the red squares. Bottom row, from the left: (1) Overview image from 7 August 2010. (2-4) Detail of the same area as middle row, from the dates 23 August 2011, 1 September 2011, and 9 September 2011.

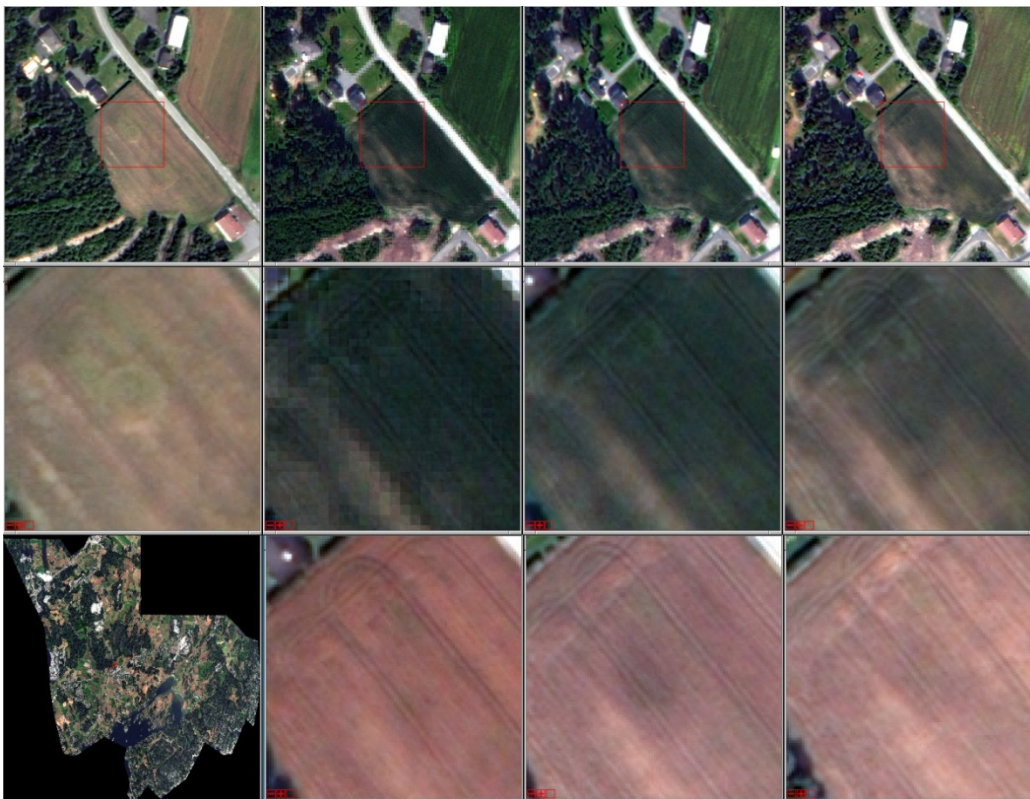


Figure 26. Time series of Worldview-2 images of crop mark at Huseby. The figure is organized in the same way as Figure 25.

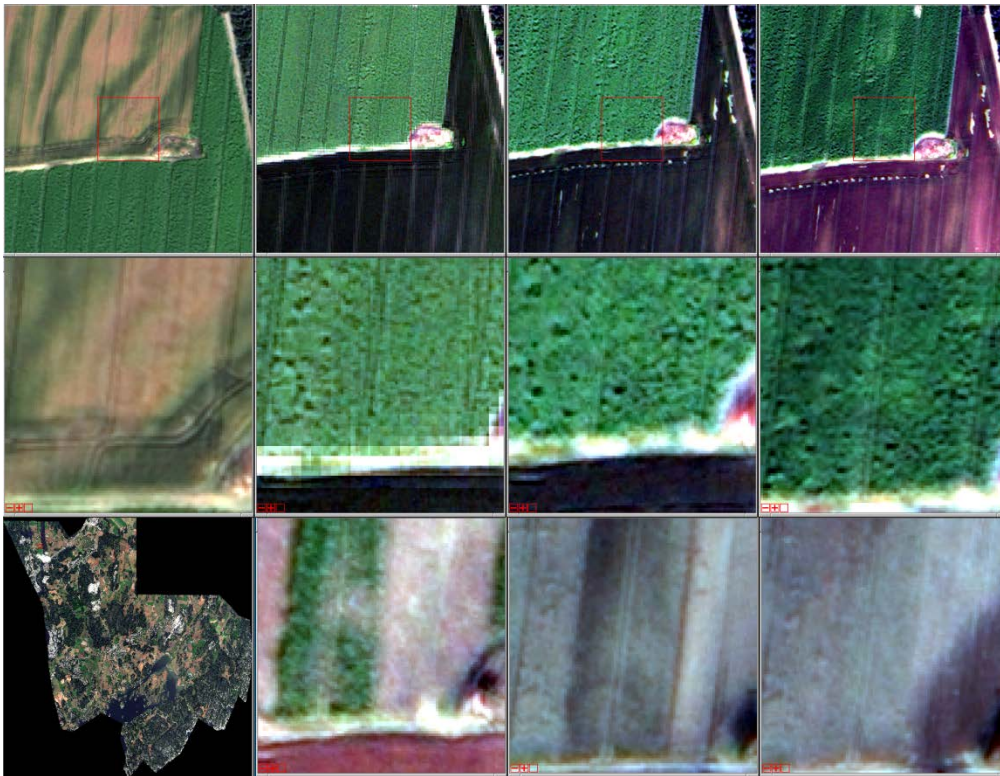


Figure 27. Time series of another crop mark detection (561140E, 6551309N). A circular crop mark appears in the 1 September 2011 image (bottom row, no. 3 from the left), south of the 7 August 2010 crop mark.

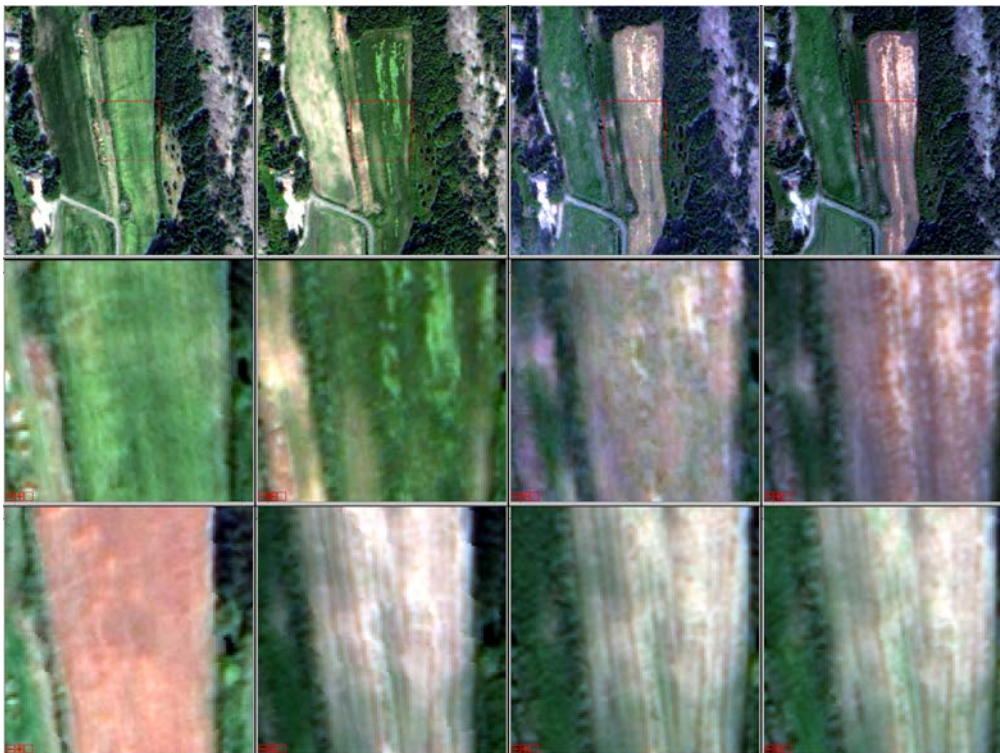


Figure 28. Time series of crop mark detection in the Brunlanes image (557901E, 6538291N). Upper row, from left to right: 16 July 2010, 11 July 2011, 27 July 2011, 2 August 2011. Middle row: detail of upper row, inside red squares. Bottom row: Detail views, from left to right: 7 August 2010, 23 August 2011, 1 September 2011, 9 September 2011. Except for the left column, the figure is organized in the same way as for the Tjølling image time series.

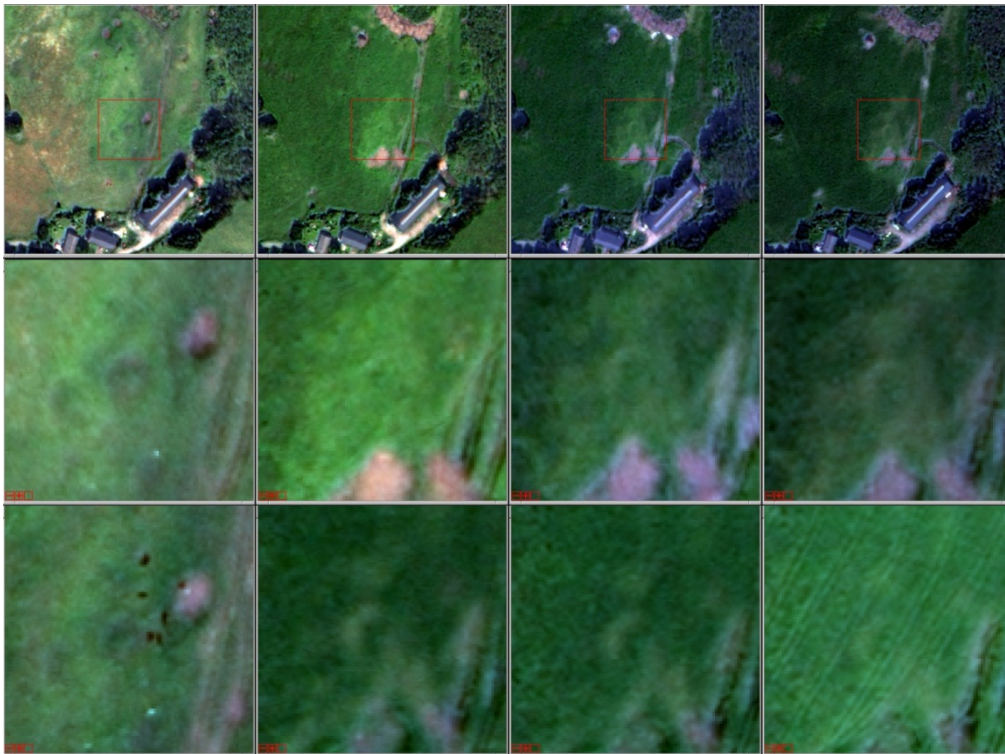


Figure 29. Time series of another crop mark detection in the Brunlanes image (556411E, 6540068N).

## 5 Field inspection of crop marks

### 5.1 Field work at Valby, Larvik, Norway – non-intrusive methods

In 2009 the project acquired Quickbird images for large areas in Vestfold. One of these images show two very strong ring shape anomalies (Figure 30) in a crop field belonging to the farm of Valby in Larvik Municipality. The positioning of these anomalies must be seen in connection to a close by Iron Age grave field (ID 38694 1-8) which in present day landscape is situated 90 meters south of the northern most found anomaly.



Figure 30. From Quickbird image of Tjølling, acquired on 24 July 2009. Two circular crop marks are clearly visible in the field south of the farm Valby, Larvik municipality, Oppland County, Norway.

The Valby site is situated close to the thing place Tjøllingvollen to the east, and also close to the Viking age city of Kaupang to the south (Figure 31). In this landscape Vestfold County Council has conducted many surveys, and this area has been a focal point for Norwegian archaeology since the early 19th century. Many sites are known and many have been excavated by both professionals and amateurs.

In connection with another project we were able to undertake a minor geophysical investigation of the field at Valby in 2011. This international project is led by *Ludwig Boltzmann Institute for Archaeological Prospection and Virtual Archaeology (LBI)*, Vienna, Austria. The project is dedicated to undertake large scale geophysical investigations in several European countries (Austria, Germany, Sweden, England and Norway). Vestfold County is an investigation area within the project and the area around Tjøllingvollen and Kaupang is a focal area in the project.

In September 2011 the LBI-led project investigated the field at Valby, both with magnetometer and high resolution georadar. We wanted to test the strong anomalies detected with

CultSearcher, to see if these also could be confirmed with geophysics, before investigating the anomalies with traditional archaeological excavation techniques.

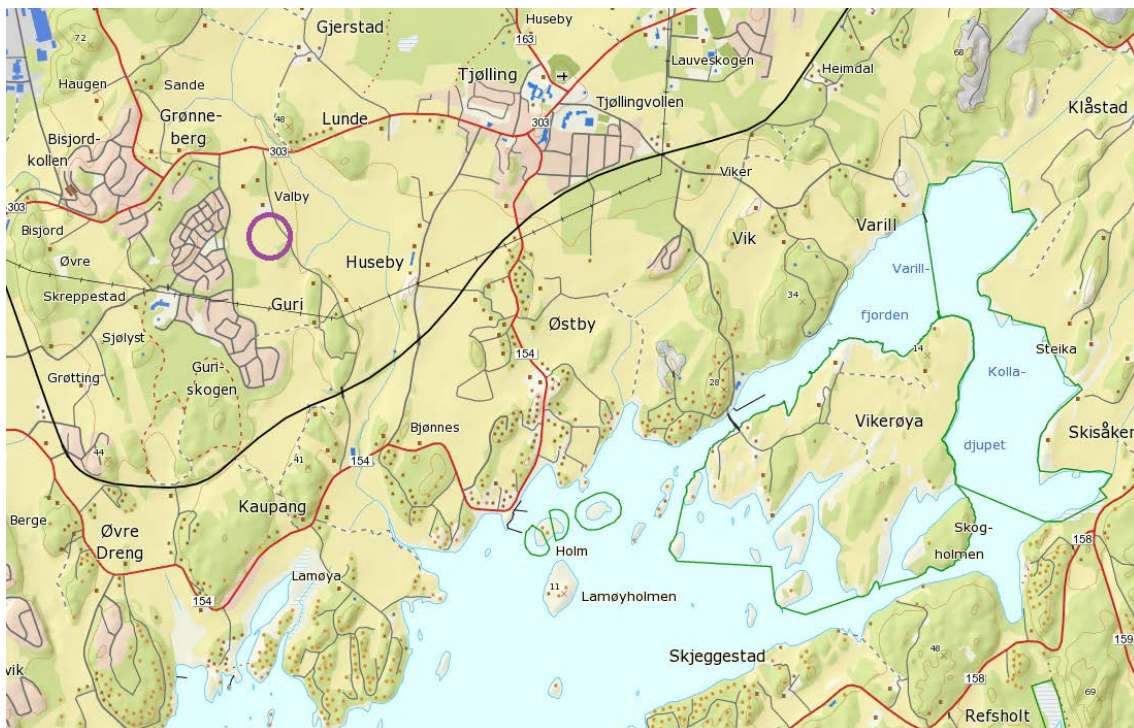


Figure 31. The field at Valby (purple circle) and surrounding landscape. Kaupang is to the south and Tjøllingvollen is to the east.



Figure 32. Part of Quickbird image from 2009. The two circular crop marks are located inside the purple circle.

The results from two days surveying with magnetometer and georadar were very convincing and confirmed the strong anomalies detected with Cultsearcher. These are probably the

remnants of over ploughed grave mounds that most likely were connected to the grave field (Askeladden ID 38694) to the south.

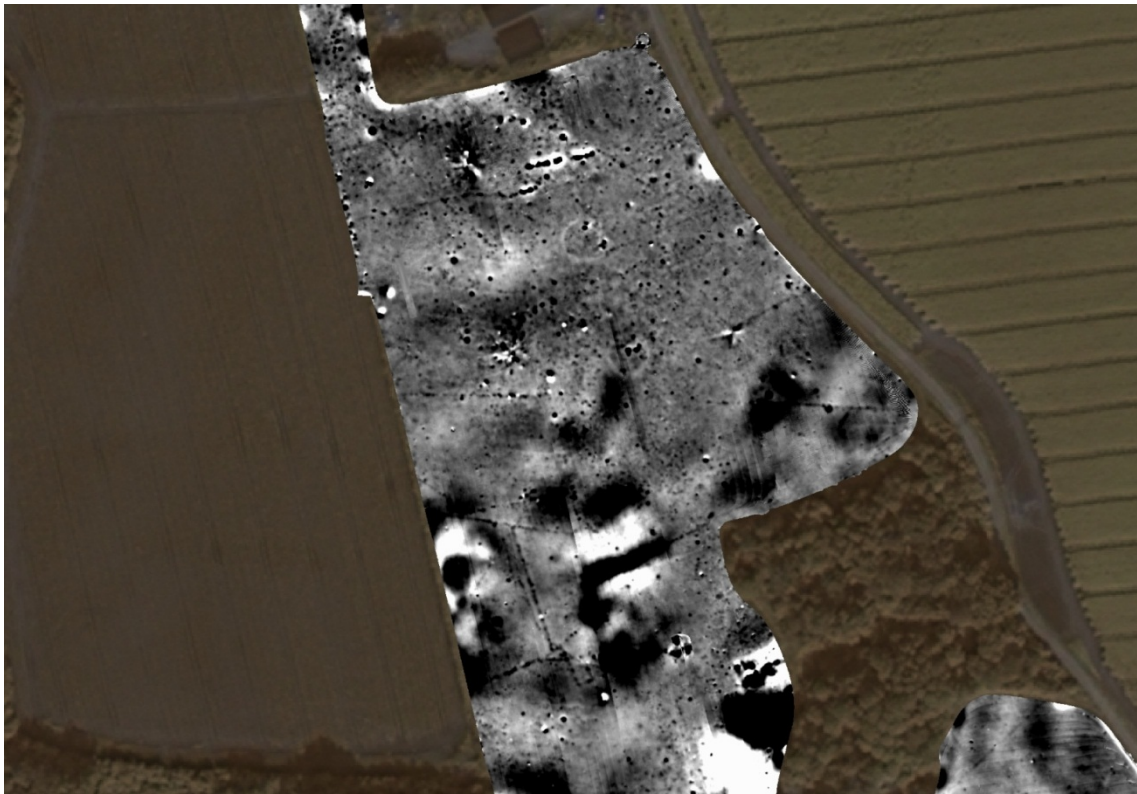


Figure 33. Result of magnetometer survey on the field south of Valby.

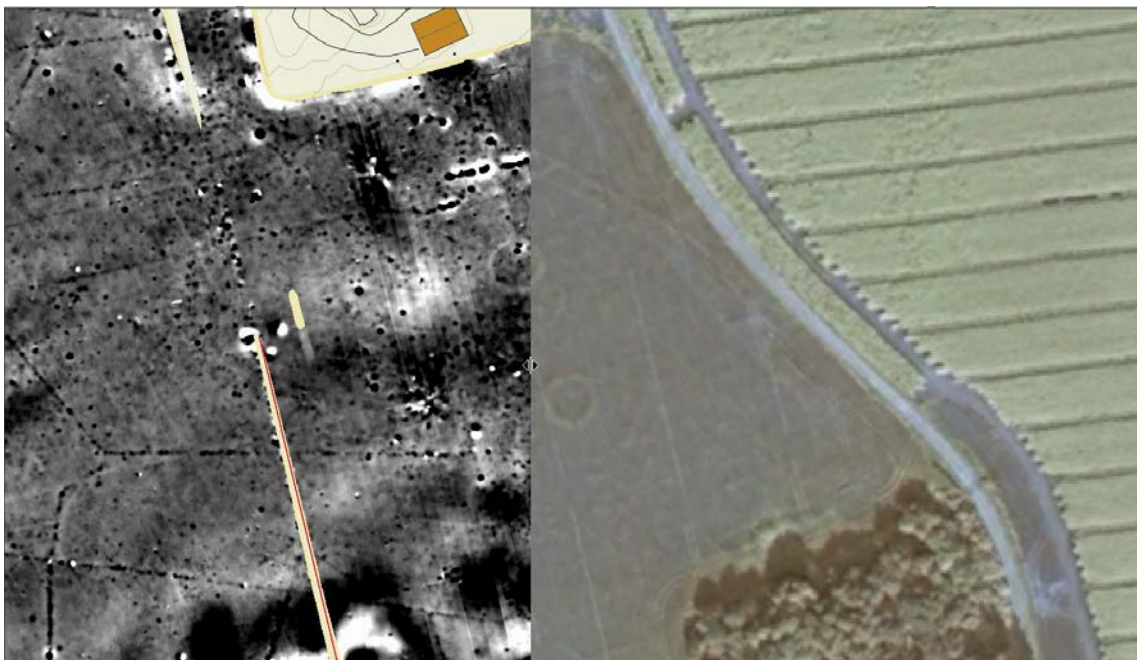


Figure 34. Composite image, with magnetometer data to the left while the Quickbird image is being peeled away towards the right. The magnetometer data is showing a perfect match to the satellite image detections.

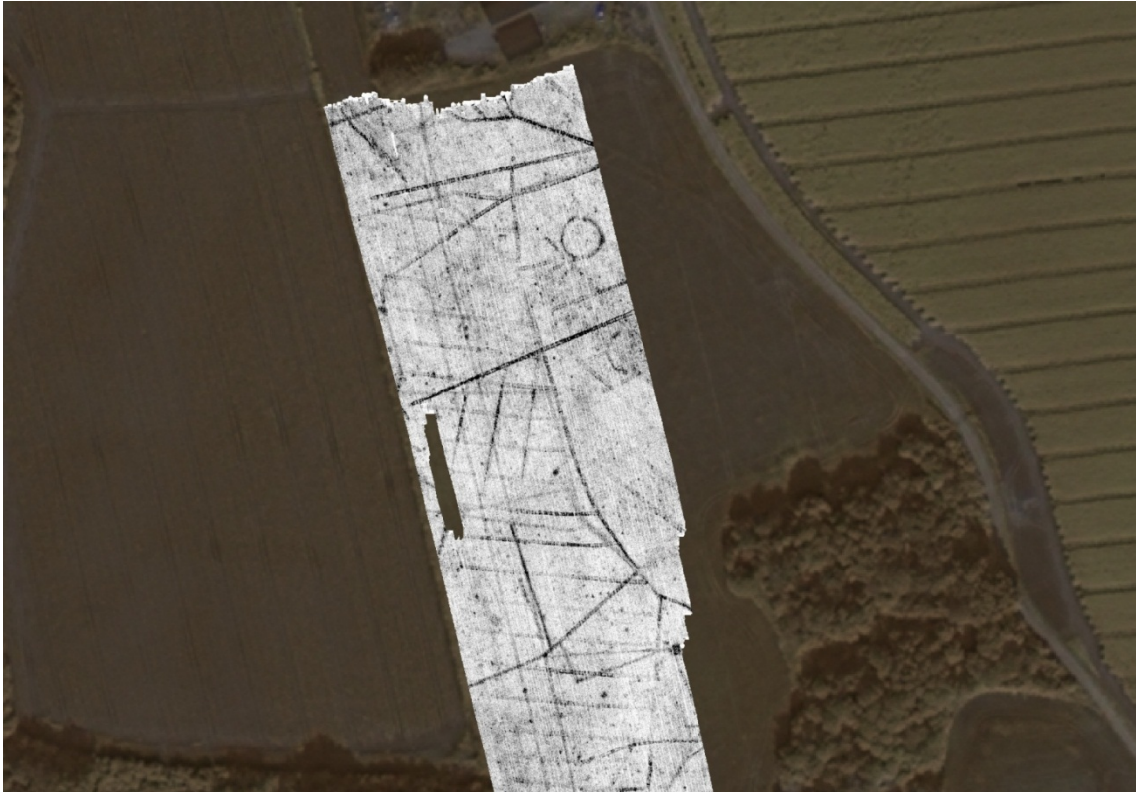


Figure 35. Result of ground penetrating radar on the field south of Valby.

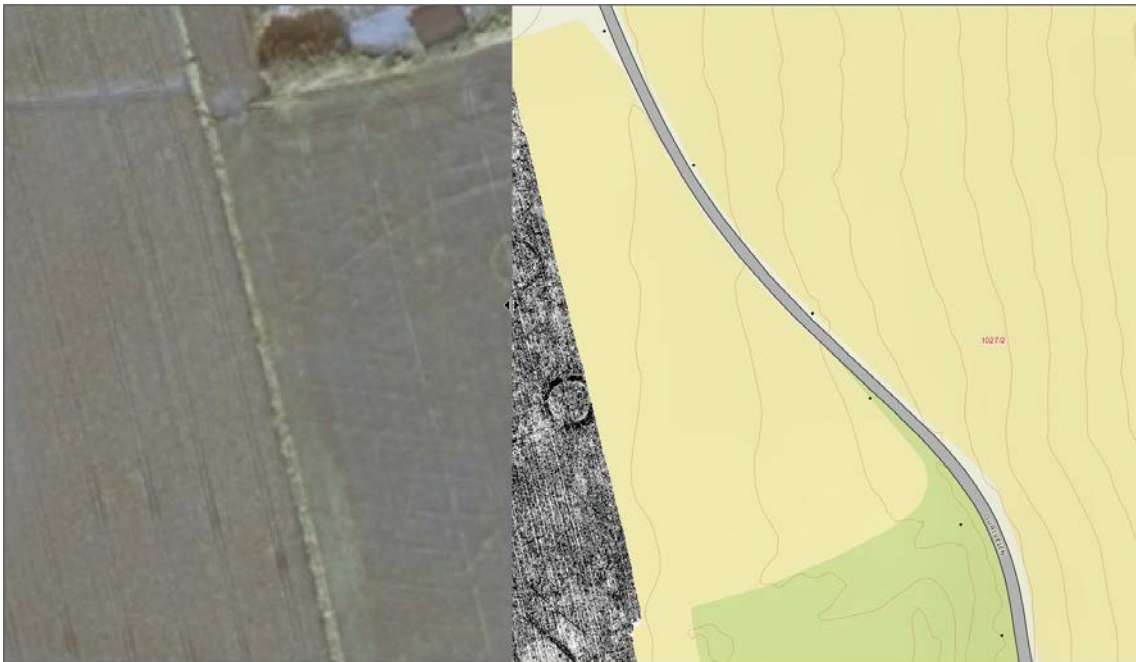


Figure 36. Composite image, with the Quickbird image to the left, being peeled towards the left unveiling the results from the georadar survey, again perfect match with the anomalies.

While these non-intrusive surveys give a strong indication of two levelled grave mounds, we wanted to further confirm our results by using traditional archaeological fieldwork. This was done for two reasons:

1. to get clear physical evidence for using these new methodological approaches, and
2. to get a clear view of what is actually left of the archaeological feature.

## 5.2 Results, small scale archaeological excavation at Valby

On 25 October 2011, a small scale archaeological excavation was performed on the field (Figure 37) south of the farm Valby, Larvik Municipality. We opened two small trenches crossing the supposed ring ditch of the northernmost of the two anomalies that were present both in the Quickbird image (Figure 30) and in the geophysical data (Figure 33-Figure 36). In a digital map, two rectangular trenches were overlaid the georadar and Quickbird images for the northernmost ring ditch (Figure 38). By using an Altus RTK CPOS GPS (Figure 39) and this map overlay, the corners of the trenches were located in the field. Before opening up the areas with an excavator, the entire area on top of the ring ditch was surveyed with a metal detector. Then, the trenches were dug by removing a 10 cm deep layer of soil at a time (Figure 40). Each time a layer of soil was removed, the metal detector survey was repeated for the trench area (Figure 41). In total, this resulted in finding 94 artefacts; most of these were quite modern objects, but a few iron objects will be further investigated.



Figure 37. The field at Valby before excavation, looking towards the south.

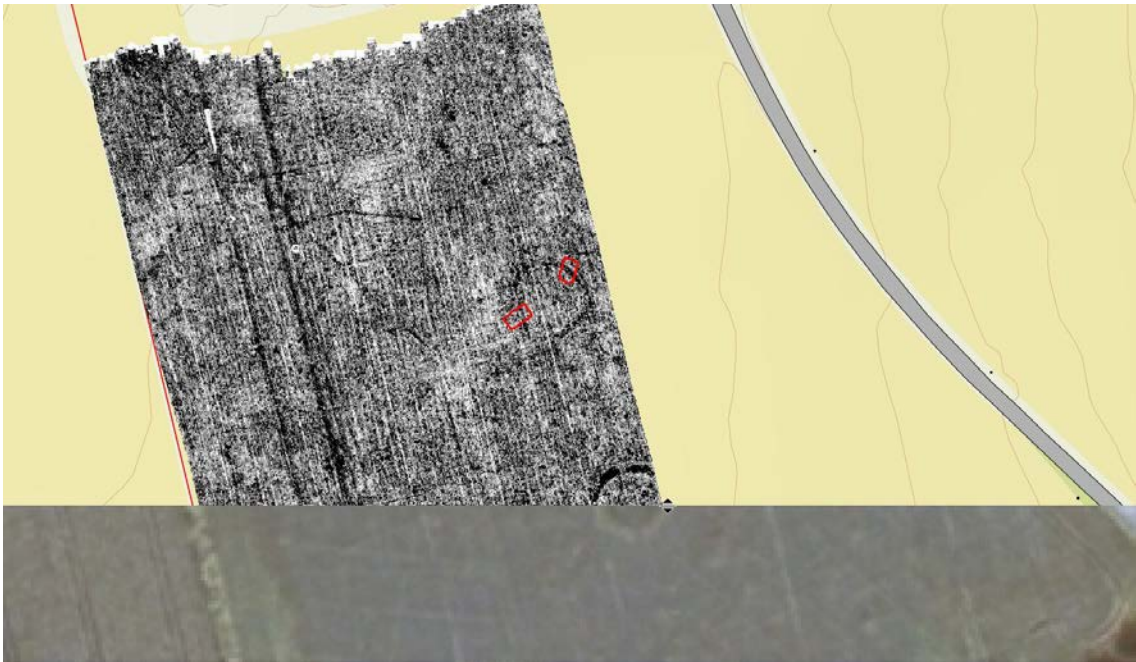


Figure 38. The placement of two trenches across the northernmost ring ditch.



Figure 39. The corners of the planned trenches were located accurately using GPS and map overlays.



Figure 40. The top soil was removed, 10 cm at a time.



Figure 41. After each time 10 cm of soil was removed, metal artefacts were found using a metal detector.

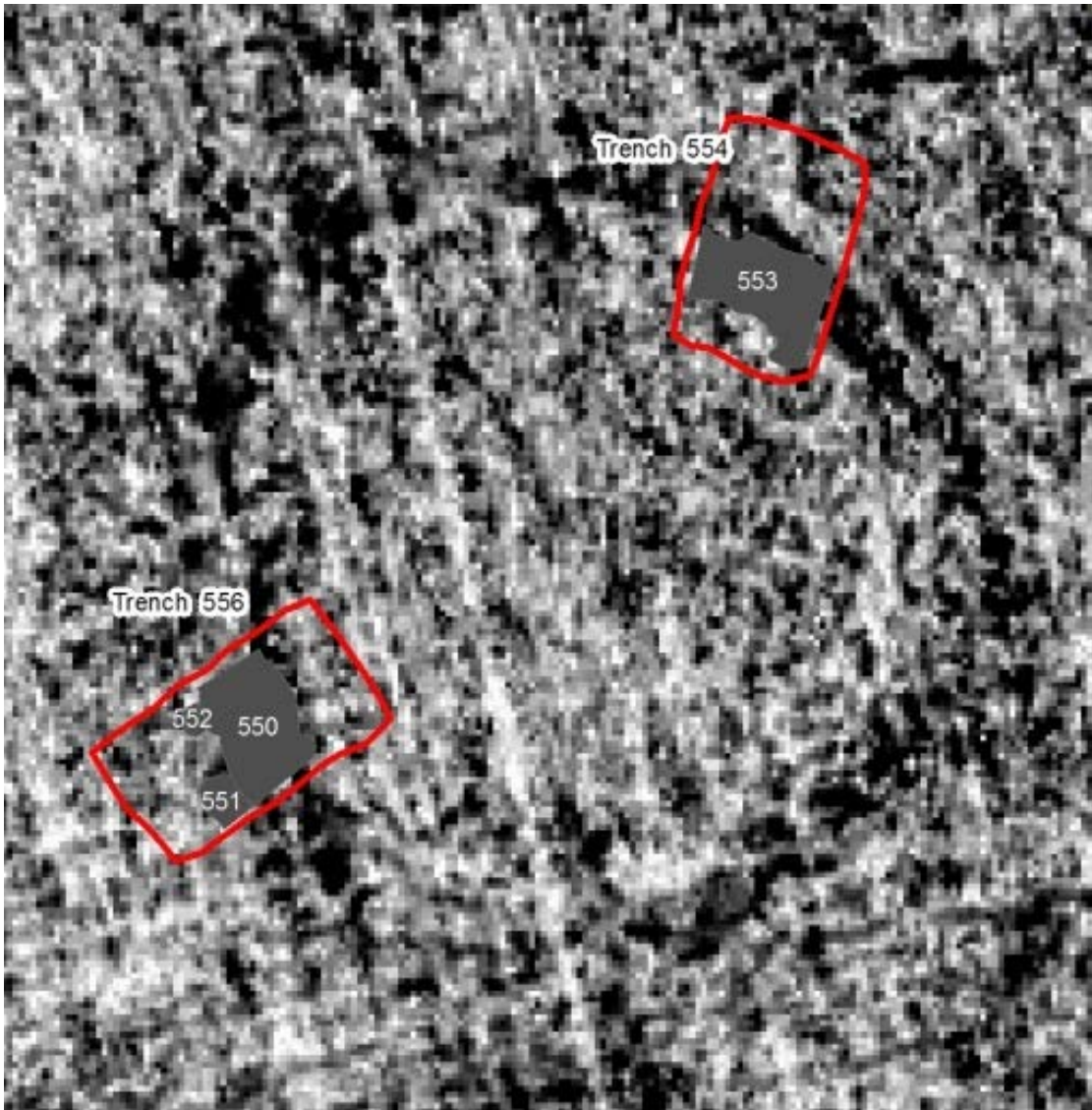


Figure 42. The two trenches 554 and 556 (red squares) and the two discovered remnants of the ring ditch (grey areas).



Figure 43. Below 30 cm of top soil, the ring ditch appears.



Figure 44. Cutting a small cross section through the ring ditch.



Figure 45. Cross section of ditch. The ditch is surrounded by gravel and sand. The ditch itself is filled with a different, very fine grained material.

The area of the trench 554 measured 2.4 m x 3.7 m, and the trench 556 measured 2.5 m x 4.5 m (Figure 42). We started by digging trench 556. Below 30 cm of soil, the ring ditch appeared as a 2 meter wide stripe with soft, dark grey anthropogenic masses, containing some charcoal and small pieces of burnt clay (Figure 43). The surrounding natural subsoil consists of heterogeneous moraine masses, containing sandy belts, and rock/pebbles, yellow to orange in colour.

After digging trench 556 and successfully finding the ring ditch, we opened up trench 554. This part of the ring ditch also appeared under 30 cm of soil. It was a bit less obvious than in trench 556, and it was situated in more soft sandy subsoil.

In order to record the actual preservation of the ring ditch a cross section of the ring ditch was dug in trench 556 (Figure 44).

The sectioning of the ring ditch A550 in trench 556 (Figure 45) showed that the feature was well preserved and continued down by another 35 cm. Two C-14 samples were collected from the profile.

### 5.2.1 Concluding remarks

The investigations at Valby showed that the combination of non-intrusive surveying methods may give convincing evidence of the presence of levelled grave mounds. This offers archaeologists unique opportunities for conducting a much better planned excavation with key-hole trenching. Further, the use of non-intrusive methods opens up a possibility for surveying larger areas where we until now only have used traditional excavation methods.

### 5.3 Geophysical survey of crop marks at Store Sandnes



Figure 46. Three circular crop mark detections in the Worldview-2 satellite image of Tjølling of 7 August 2010, at Store Sandnes.



Figure 47. One of the circular crop marks in the satellite image of 2010 (Figure 46) is also clearly visible in the aerial ortophoto of 15 July 2002.



Figure 48. Oblique aerial photo of unknown date available from [www.gulesider.no](http://www.gulesider.no) (Norwegian "yellow pages" telephone directory.) Copyright Eniro Norge AS, Blom Geomatics AS.

### 5.3.1 Introduction

In early November 2011 NIKU conducted a geophysical survey of a site previously detected in the Worldview-2 satellite image from 7 August 2010 (Figure 46). The crop marks are also visible in scanned analogue vertical orthophoto from 15 July 2002 (Figure 47) and oblique digital aerial photo available from the website [gulesider.no](http://www.gulesider.no) (Figure 48). The survey was carried out with the assistance of staff from Vestfold County Council and the Norwegian Computing Centre. The site was centred on crop marks observed in the satellite imagery. These consisted of three well-defined circular features of roughly equal dimensions. Within one of these features a smaller, circular feature could be discerned. The three features have been interpreted as ring ditches from ploughed out burial mounds, and the central feature has been interpreted as the remains of a grave. The aim of the project therefore was to investigate whether the use of geophysical methods could further define the features, to estimate their depth, and to determine their current level of preservation.

### 5.3.2 Site description and survey

The site is located approximately 250m southwest of the farm Store Sandnes in Sandefjord, and consists of a cultivated field sloping gently towards the southeast. The area had been harvested prior to the geophysical survey, and the field consisted of relatively even crop stubble. Due to the large amounts of precipitation experienced in this part of the country during the 2011 autumn, the surface of the site was partly disturbed by tractor and other machine tracks. This affected the progress of the survey somewhat and a small section of one of the two survey areas had to be left out of the survey.

Two areas were surveyed on 9 and 10 November 2011 (Figure 49). Survey area A was located in the westernmost corner of the field. It measured 20m x 30m (600 m<sup>2</sup>), and was orientated NE-SW. The area was staked out arbitrarily to investigate whether any features connected with those in the satellite image could be detected. Survey area B was located to the southeast of

Survey area A. It was square in shape with 50m sides, apart from an area of 165m<sup>2</sup> to the northwest which was avoided on account of the previously mentioned machine tracks. Survey area B therefore measured 2335m<sup>2</sup> in total. The area was staked out in advance, centred on the crop marks observed in the satellite imagery.

### 5.3.3 Method and instrumentation

The survey areas were staked out using a real time kinematic (RTK) GPS system, and survey tapes were stretched out between the southernmost and northernmost survey points. These acted as start and stop lines for the survey. Additionally, sturdy lines were stretched out between the survey tapes to act as guidance lines for walking the transects. The survey itself was carried out using a Sensors and Software Noggin 500 Plus single-channel geo-radar, which consists of a 500 MHz centre frequency antenna mounted on a wheeled cart configuration. The frequency range of these systems provides an ideal compromise between dataset resolution and depth penetration, and depending on the soil conditions it can generate three-dimensional information of the subsurface down to a depth of 2-3m. The distance between each transect was 25cm and the instrument was set to record return signals every 2.5cm along the transects.

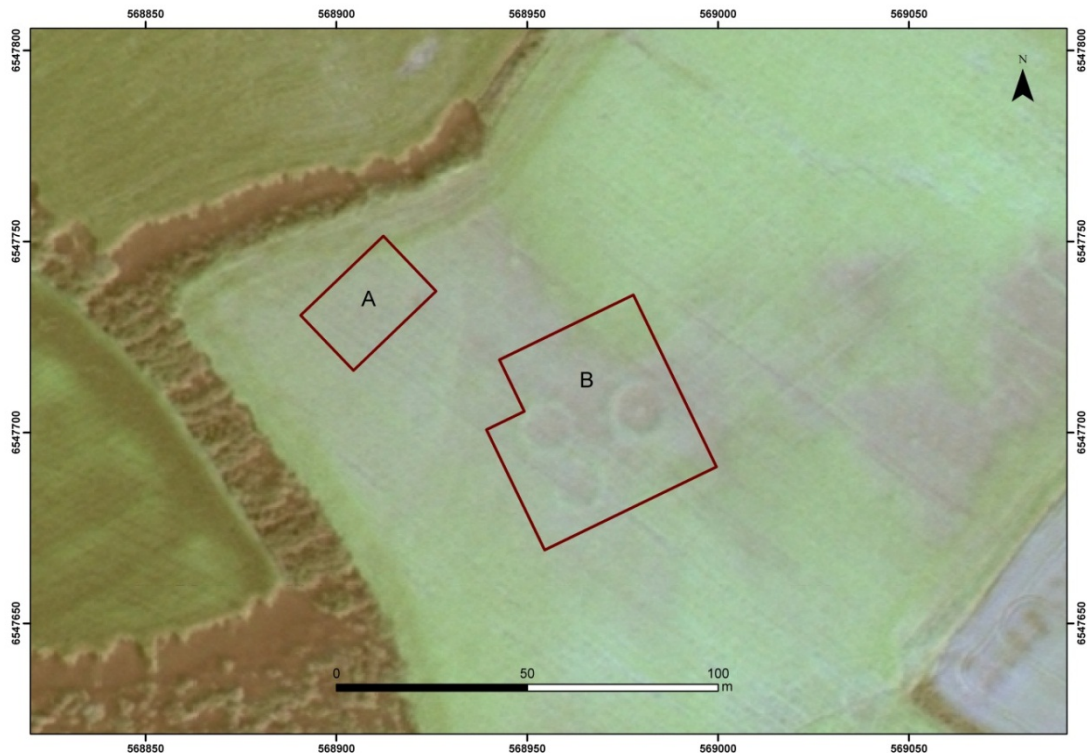


Figure 49. The survey areas superimposed on the satellite image of 7 August 2010.

### 5.3.4 Results

No anomalies of archaeological interest were observed within Survey area A. A single drainage ditch could however be seen crossing from NW to SE in the south-western part of the area (Figure 50-Figure 51). The penetration depth of the radar signals in this area extends to approximately 1m, with the features first appearing at a depth of approximately 30-40cm, which is consistent with the average plough depth in the area.

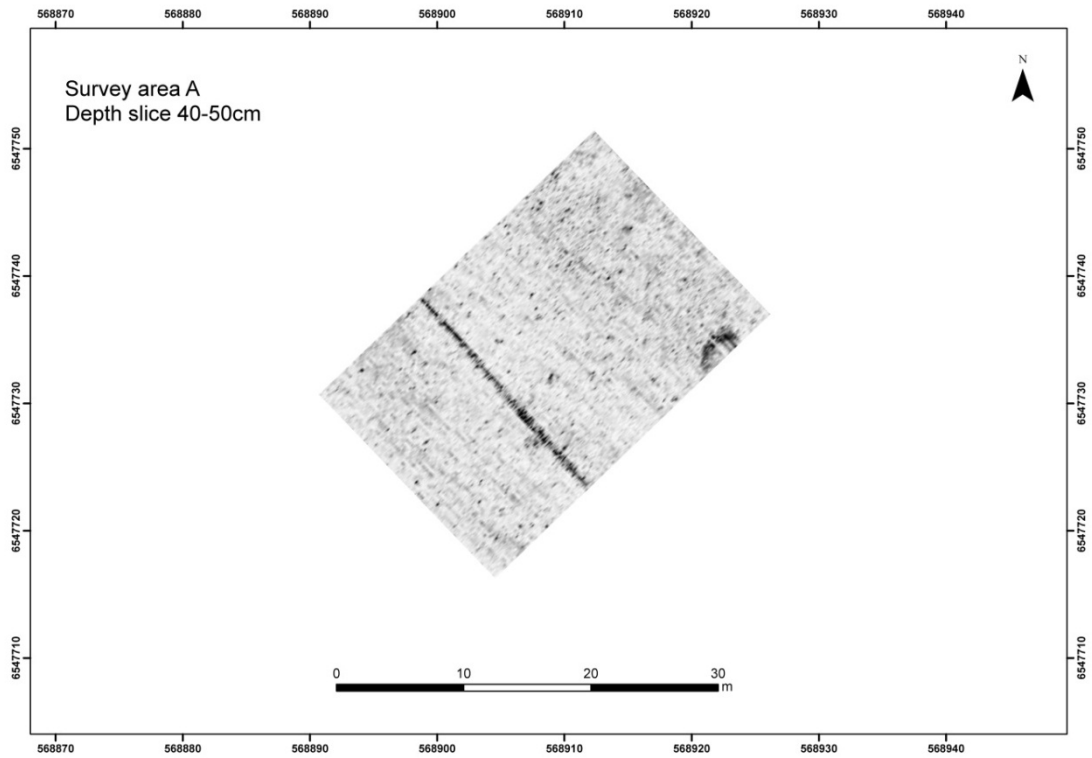


Figure 50. Survey area A. Depth slice 40-50cm.

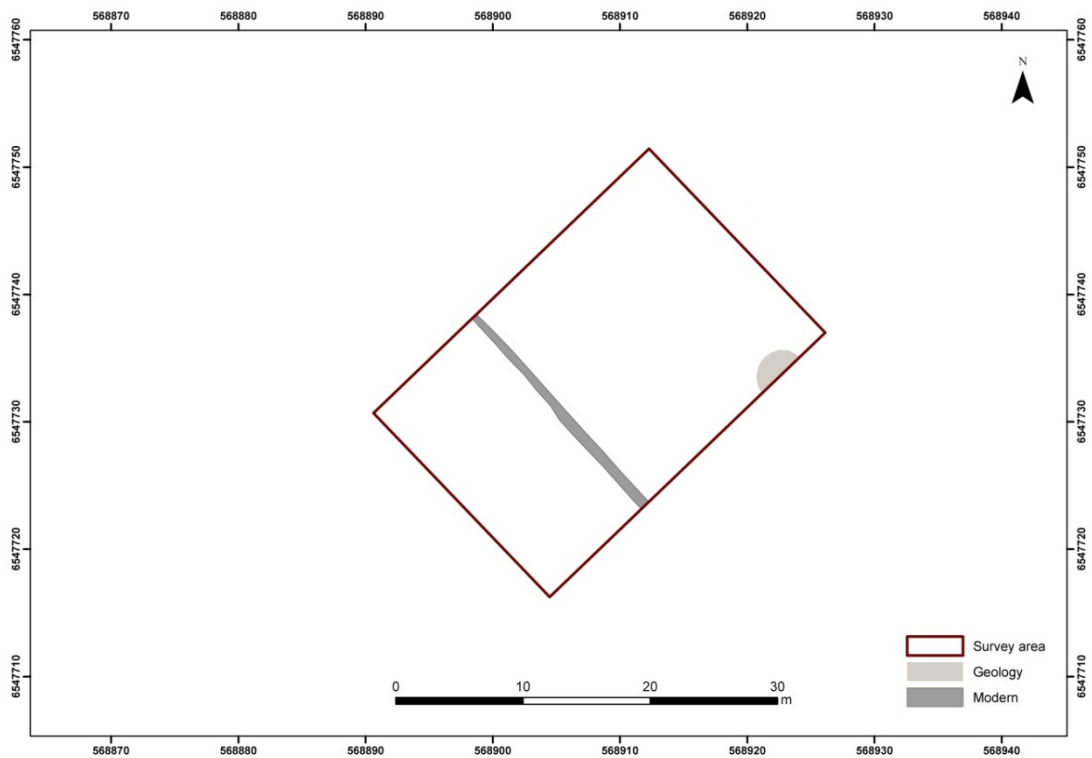


Figure 51. Survey area A. Interpretation of anomalies.

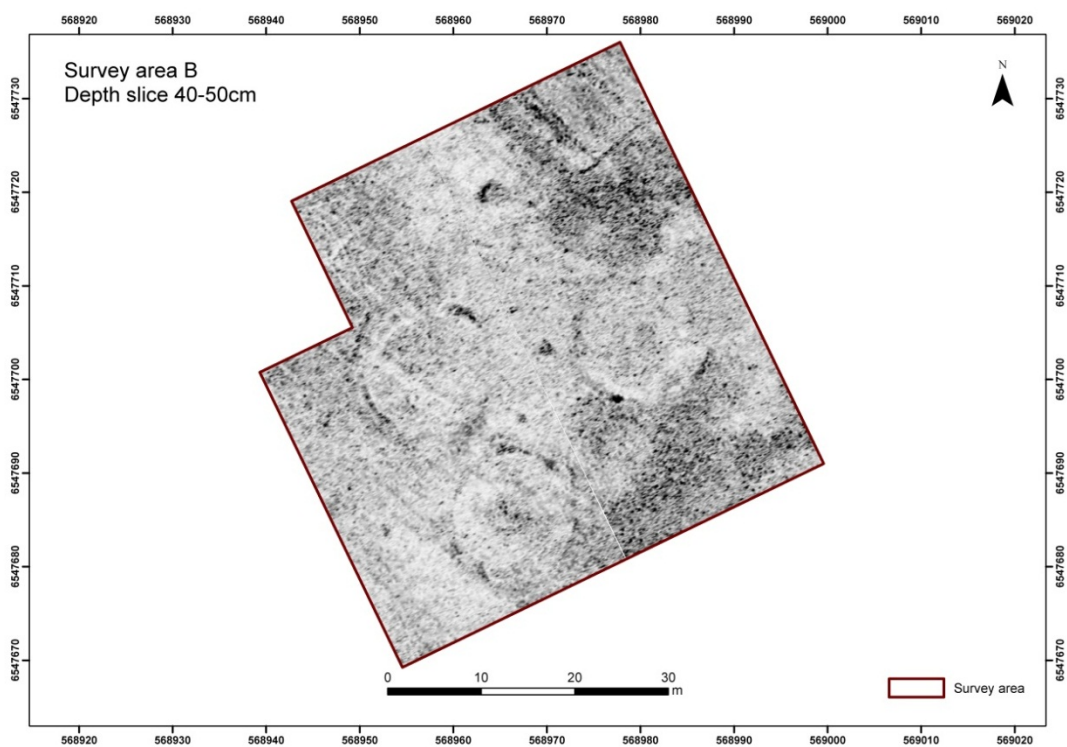


Figure 52. Survey area B. Depth slice 40-50 cm.

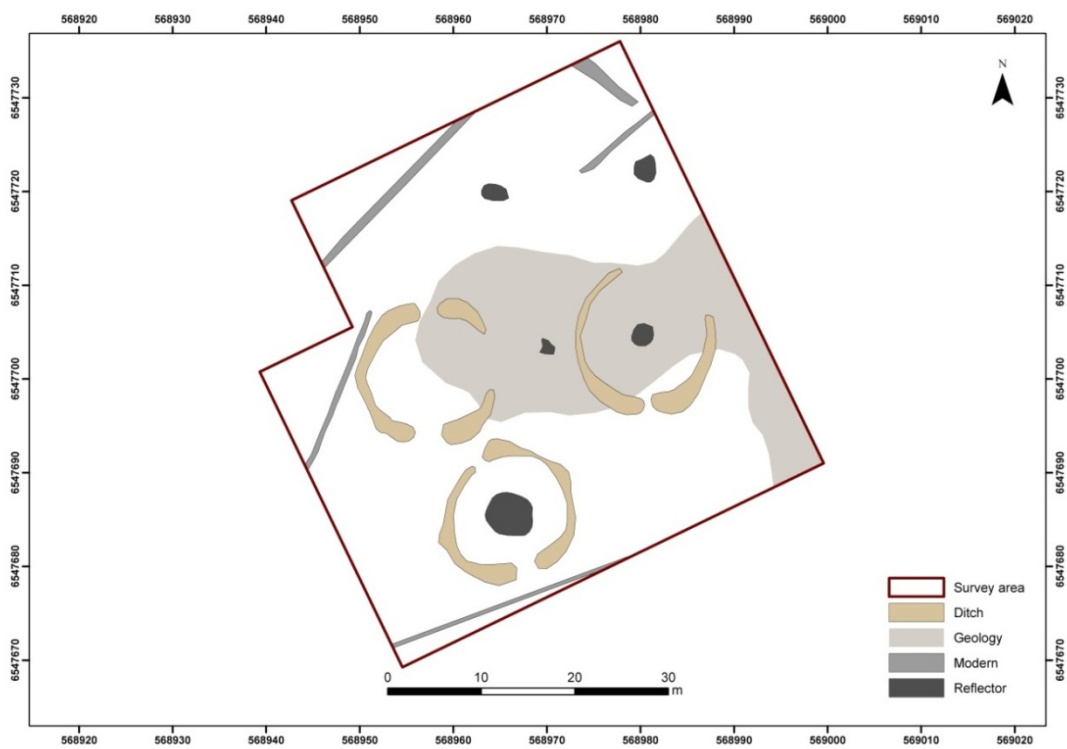


Figure 53. Survey area B. Interpretation of anomalies.

Within Survey area B a number of narrow, E-W orientated linear features could be observed (Figure 53). These have been interpreted as modern drainage ditches or pipes. The three targeted ring ditches appear in the dataset at calculated depths of between 30 and 50cm. They are all well-defined, and appear to be fairly uniform. The dataset indicates that rather than being continuous, the features all have openings to the north and south, not an uncommon feature in funerary monuments of this type. The outer diameter of the features measures between 15 and 16m, and the width of the ditches vary between 1 and 2.9m. Of the three features the southernmost appears to be the most intact. In the two northernmost features, the ditches appear to be discontinuous to the east and northeast. Although this might reflect the differing geology in this area, it is more likely to indicate the features' state of preservation. The central spot observed in the north-eastern feature in the satellite image, can also be seen in the radargrams (Figure 52-Figure 53). It is circular in shape and has a diameter of approximately 2.8m. A further circular anomaly can be observed in the radar data, within the southernmost ring ditch. This feature, which cannot be observed in the satellite imagery, is roughly circular in shape and it measures approximately 5m in diameter. It has been interpreted as the remains of a central grave.

A number of other anomalies could also be observed in the dataset. These consist of amorphous, but clearly defined features to the north of and in between the northernmost anomalies. The features measure between 2 and 3m in extent and occur at the same depth as the other features. It is not known whether these anomalies form part of other, unseen funerary monuments, or if they are individual archaeological or geological features.

### **5.3.5 Discussion**

The geophysical survey of the site at Store Sandnes yielded further information about the character, form and depth, as well as the preservation status of the features previously detected in satellite images. The features within the main survey area appear to be fairly uniform in terms of size and depth, and the geo-radar survey has confirmed the presence of a central feature within one of the northernmost ditches. Additionally, it has demonstrated the presence of a similar, hitherto unknown central feature within the southernmost ring ditch.

### **5.3.6 Remarks**

In the course of working with the satellite imagery for this report, a fourth circular feature was detected visually to the northeast of the three previously detected features (Figure 54-Figure 55). The feature measures 17-18m in diameter and is interpreted as the remains of a levelled burial mound.

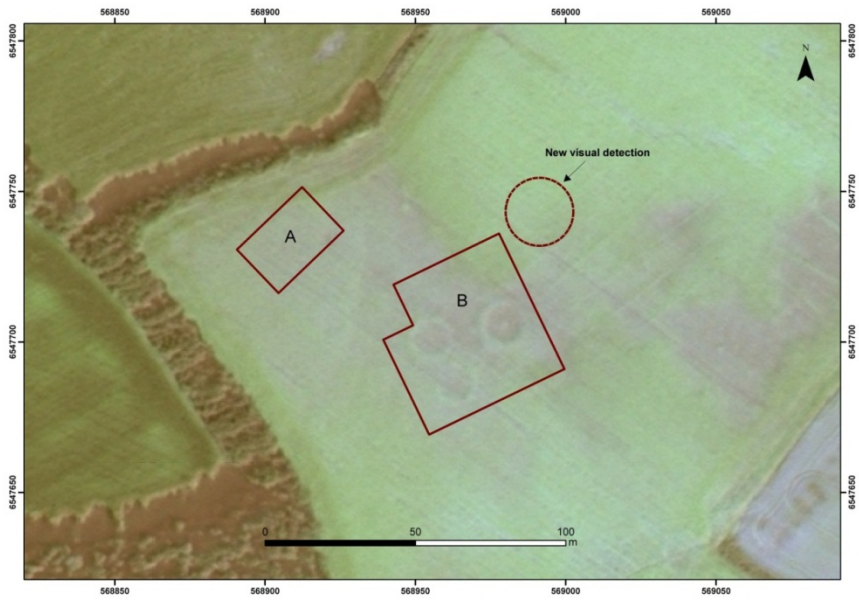


Figure 54. New visual detection (inside the dashed red circle) in the satellite image from 7 August 2010.

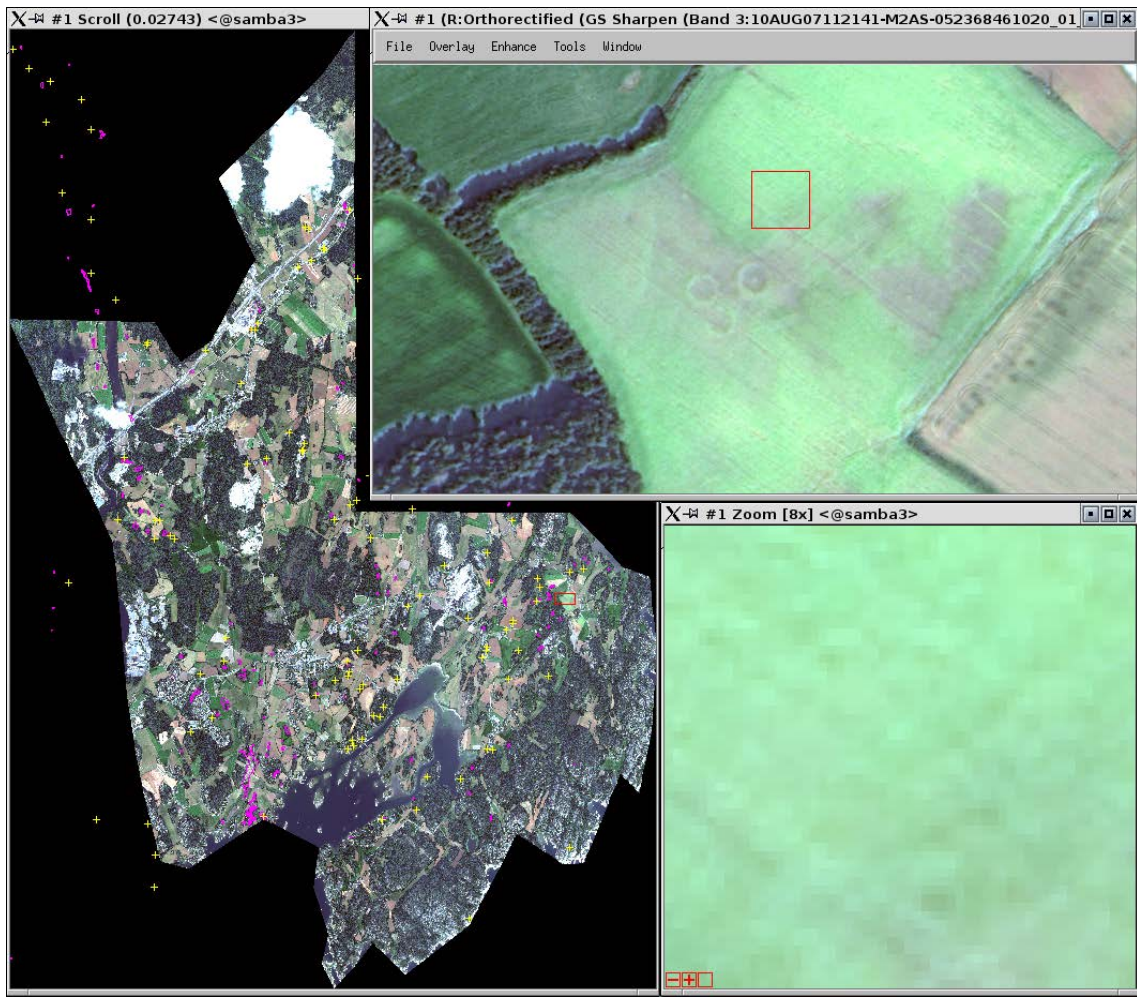


Figure 55. Bottom right: Close-up of the new visual crop mark detection at Store Sandnes. Left: Overview image of the satellite image, with grave monuments from the Askeladden cultural heritage database superimposed in pink (polygons) and yellow (points). The red rectangle indicates the portion enlarged at the top right of the figure.

## 5.4 Crop mark detections pending field verification

A number of crop mark detections were made in the 2010 Worldview-2 satellite images of selected areas in Vestfold County. The most distinct crop mark detections occurred in the Tjølling image of 7 August 2010, covering parts of Larvik municipality. This includes detections at Eide (Figure 56), Fjellvik (Figure 58) and Nedre Klåstad (Figure 60). Just out of curiosity, a preliminary version of the automatic heap detection method was run on lidar data at two of these locations. At Eide, one of the two Askeladden grave monuments was detected, with medium confidence. In addition, another heap, which could be a grave mound, was detected with medium high confidence (Figure 57). At Nedre Klåstad, one of the three Askeladden grave mounds was detected, with medium confidence (Figure 61). At Fjellvik, the visual appearance of the lidar data suggests that many false detections may be obtained in the hilly landscape (Figure 59).

There are also crop mark detections that could be worth investigating further in some of the other Worldview-2 images from 2010 (Trier et al, 2011)

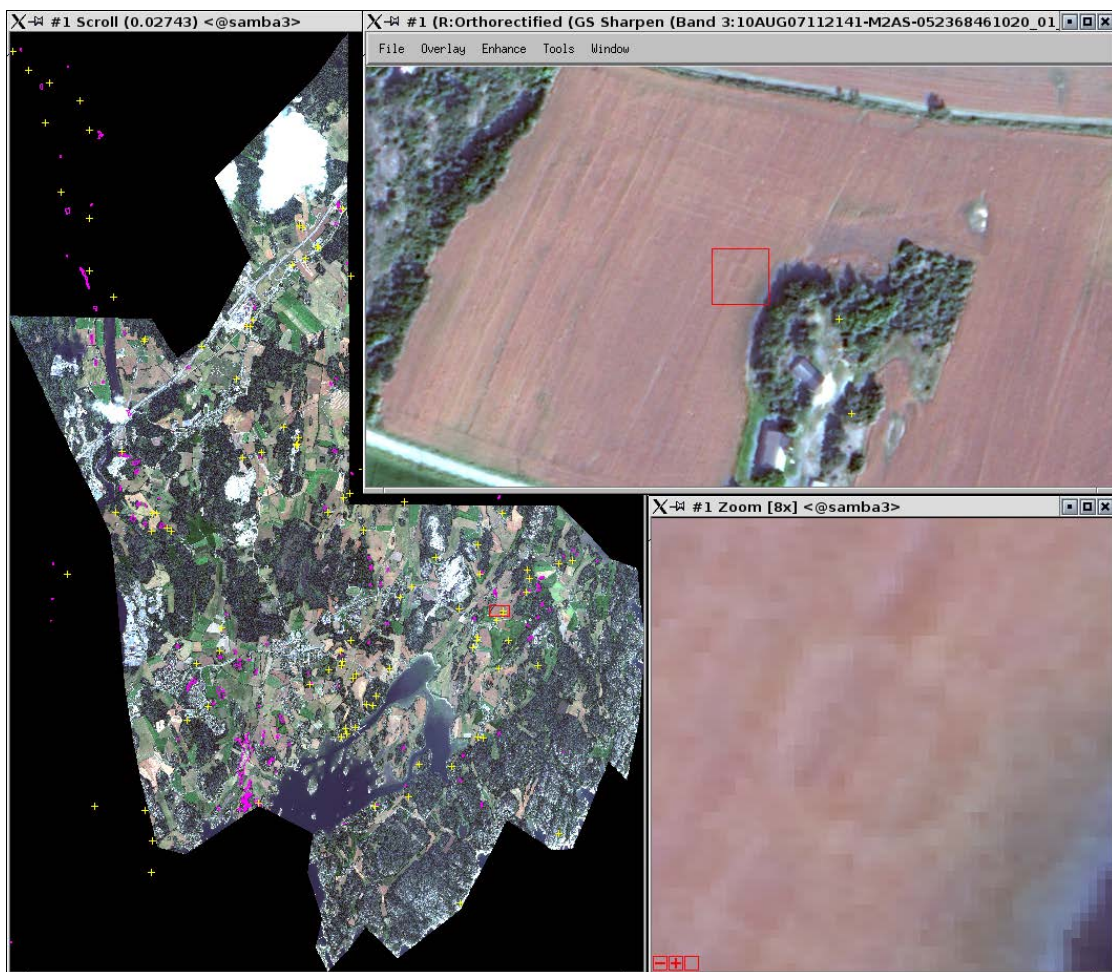


Figure 56. Crop mark detection at Eide, Larvik Municipality. In the Askeladden cultural heritage database, there are two grave mounds (yellow '+' symbols) south-east of the crop mark detection.

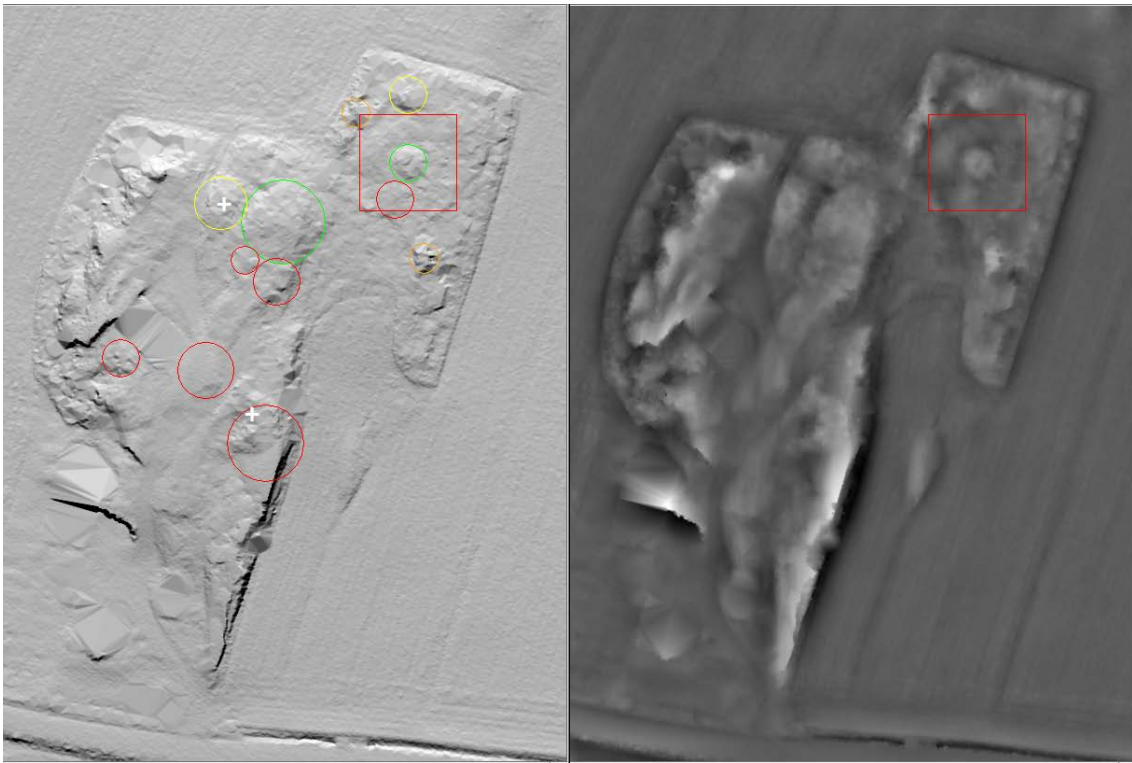


Figure 57. Automatic heap detections in lidar data at Eide. Colour codes: red circle = heap detection with low confidence, orange circle = medium low confidence, yellow circle = medium confidence, green circle = medium high confidence. White '+' = grave mound in Askeladden cultural heritage database. The red square is centred on a possible new detection of a grave mound.

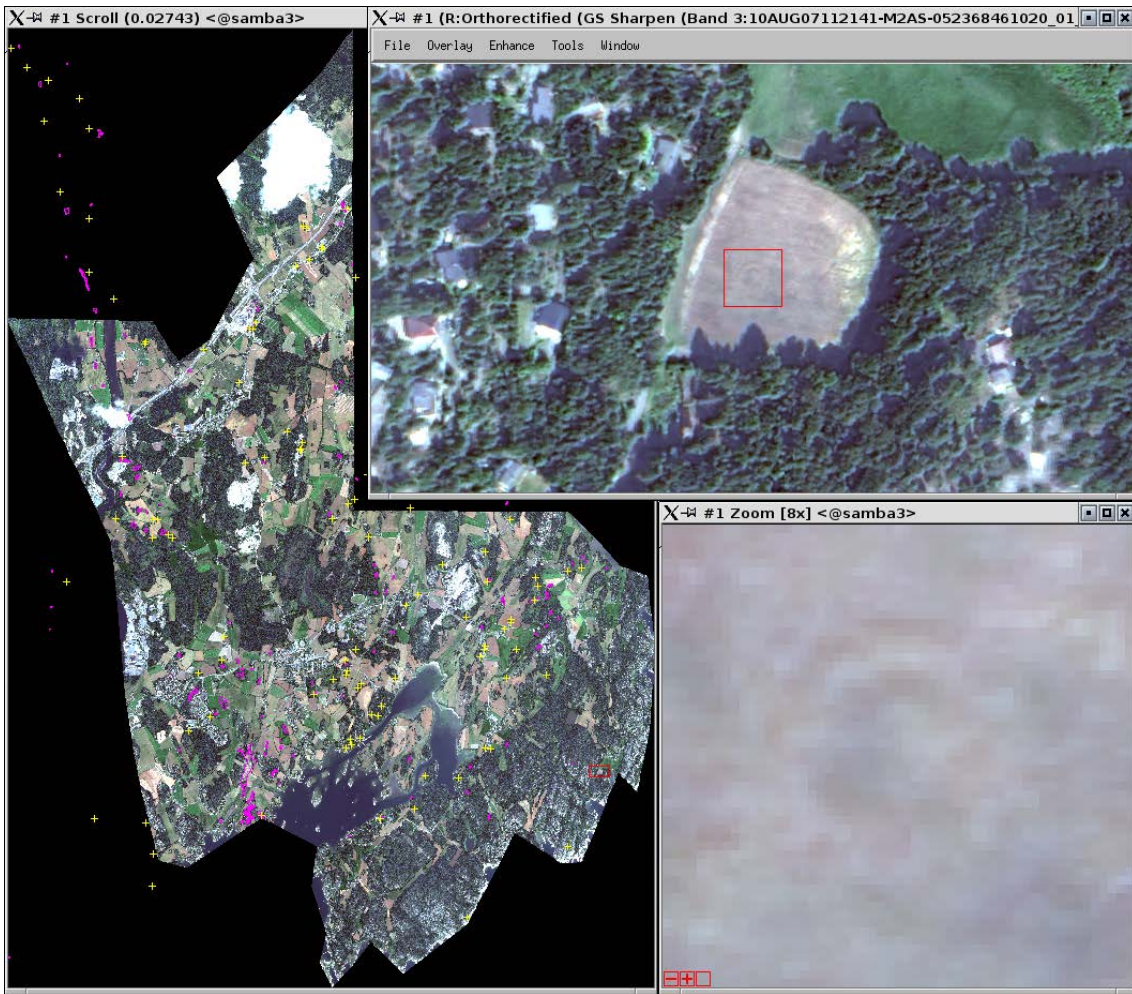


Figure 58. Crop mark detection at Fjellvik, Larvik municipality.

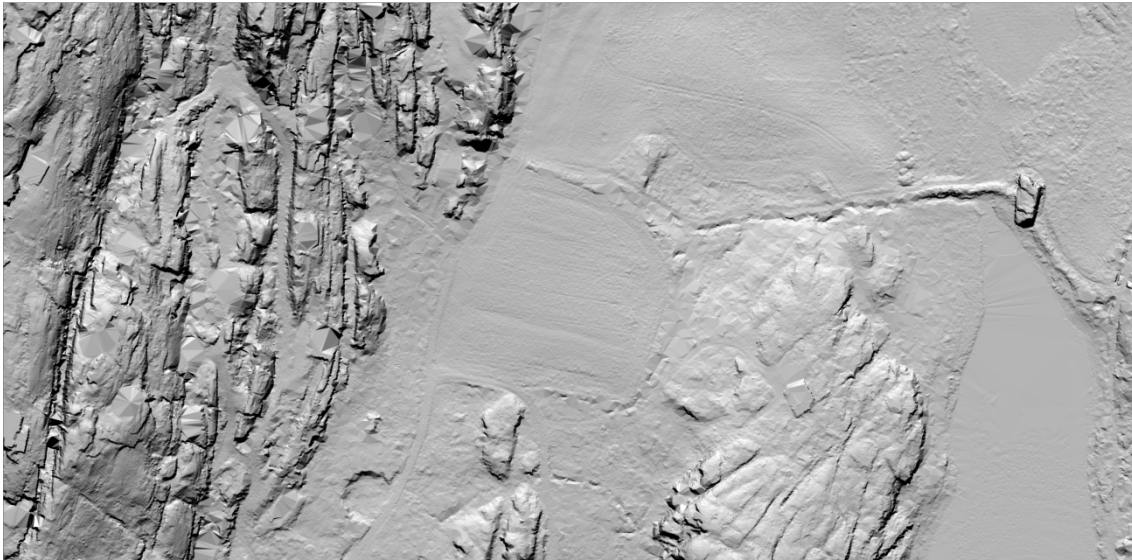


Figure 59. Lidar data from an area surrounding the crop mark detection at Fjellvik.

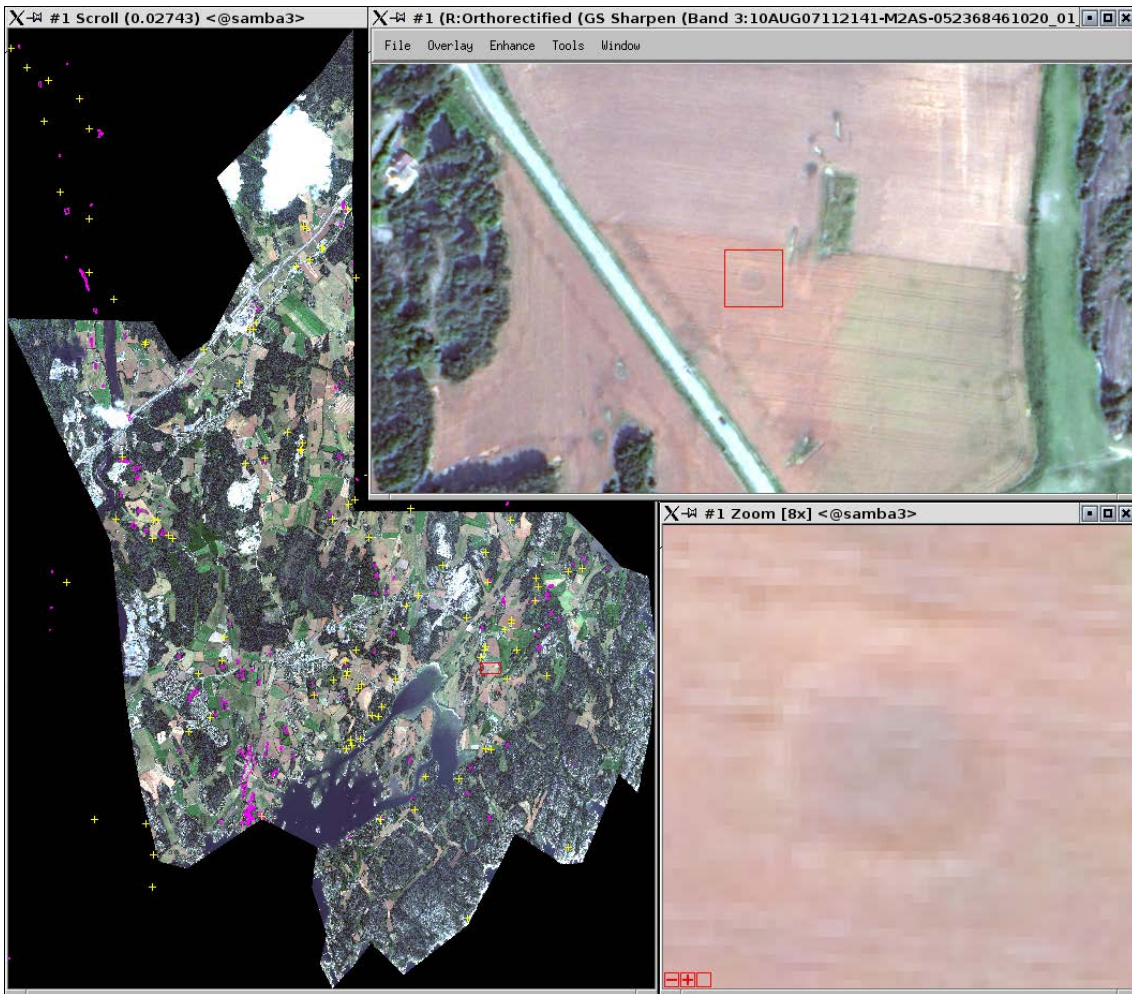


Figure 60. Crop mark detection at Nedre Klåstad, Larvik municipality.

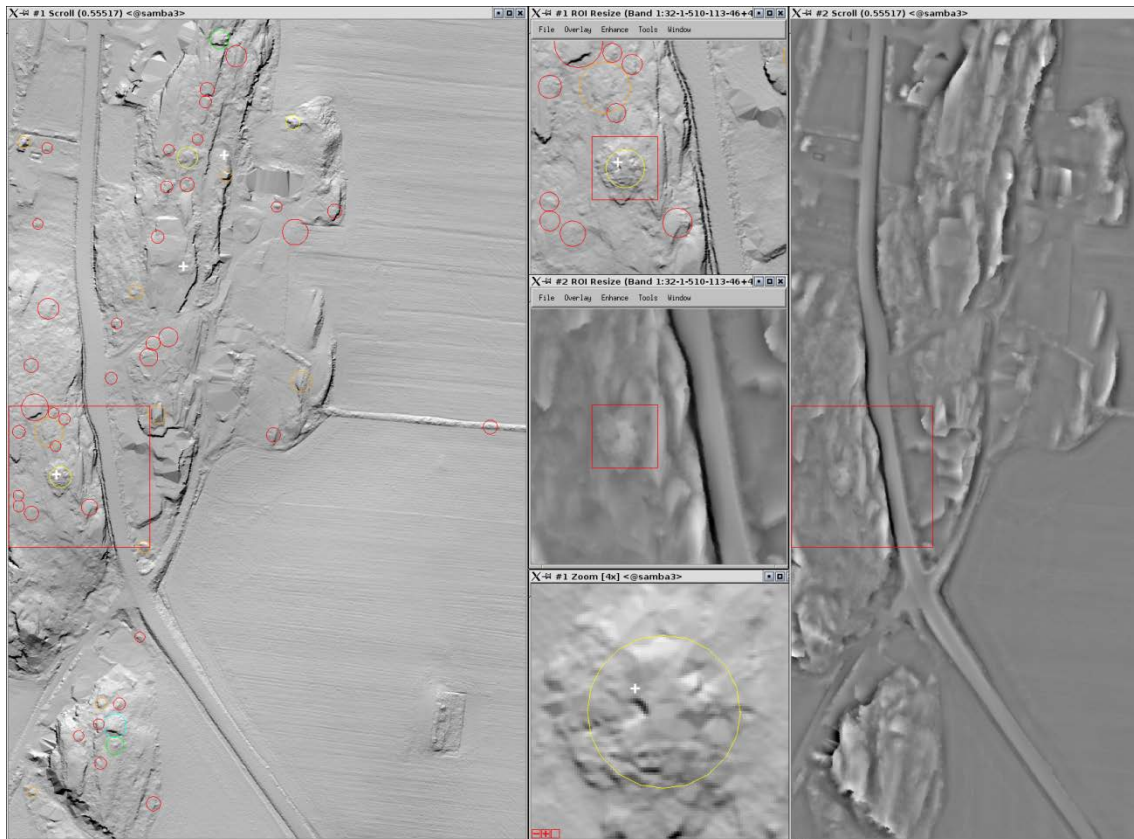


Figure 61. Automatic heap detections in lidar data at nedre Klåstad, Larvik municipality. Of the three grave mounds that appear in the Askeladden cultural heritage database, CultSearcher is able to find one of them.

## 6 Pilot portal

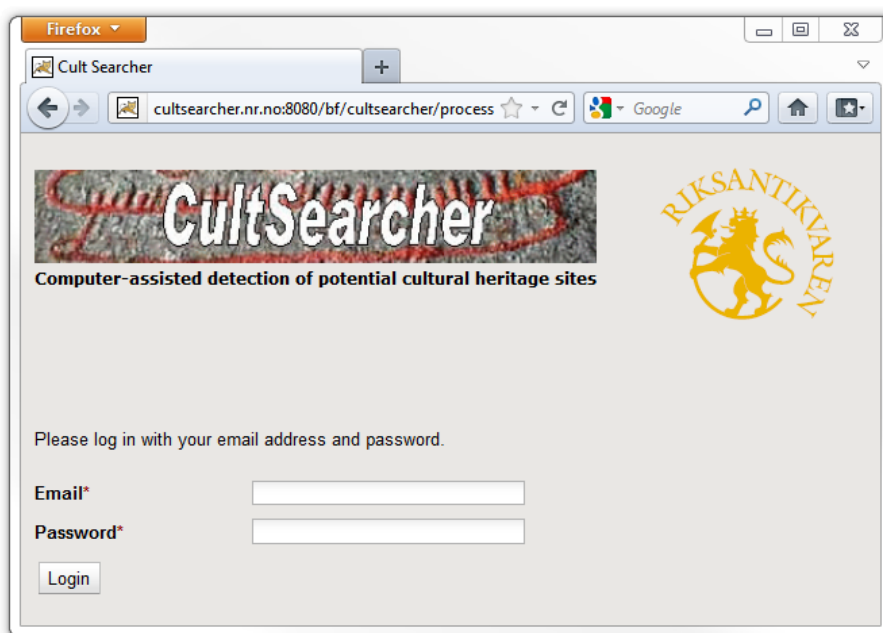
A pilot for an operational web service for the semi-automatic detection of some kinds of archaeology in airborne lidar data is currently being developed. The following description reflects the status of the development at a certain point in time in the autumn of 2011, and at the time of writing in February 2012, the portal has already changed in its appearance. However, the basic sequence of flow of data still remains the same:

1. The user logs on
2. The user transfers data
3. The web service analyses the data
4. The service emails detection results

### 6.1 Detailed description

The below description of the pilot web service is in the form of a user guide. As mentioned above, the appearance and some of the detail has already changed, so this user guide is provided merely as a reference to document what was achieved during the 2011 project year. An updated user guide will be provided when the portal is ready to be used. At the moment, there are some bugs that need to be fixed.

Open a web browser and go to: [cultsearcher.nr.no](http://cultsearcher.nr.no). The following logon screen will appear.



Type your email address and password in the spaces provided.

To obtain a password, please send an email to [cultsearcher@nr.no](mailto:cultsearcher@nr.no). Please note that only project partners will receive a password.

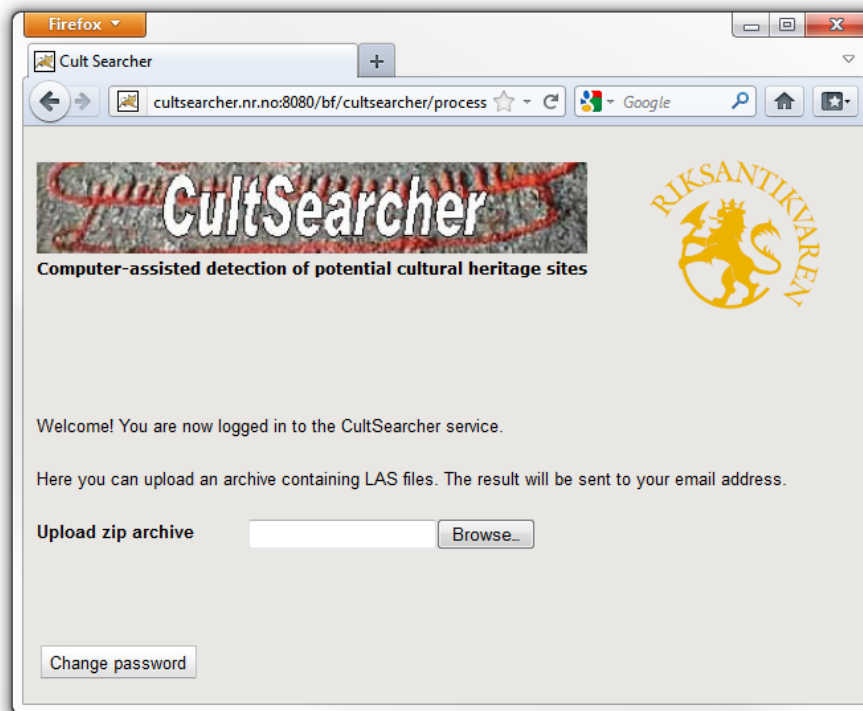
Having successfully logged in, you may now upload a zip archive containing LAS files, or you may change your password.

Each zip archive you upload and then submit for analysis will result in one set of shape files with detections. The shape files will be numbered from 1 to 6, and thus named `pit_detections_level_1`, ... `pit_detections_level_6`. The numbers 1-6 denote confidence levels, with 1 = very low, and 6=very high (Table 15). Sometimes, no detections will get the highest confidence levels, in which case the corresponding detection files will be missing, e.g., only levels 1-4 are returned.

Table 15. Confidence levels for detection results.

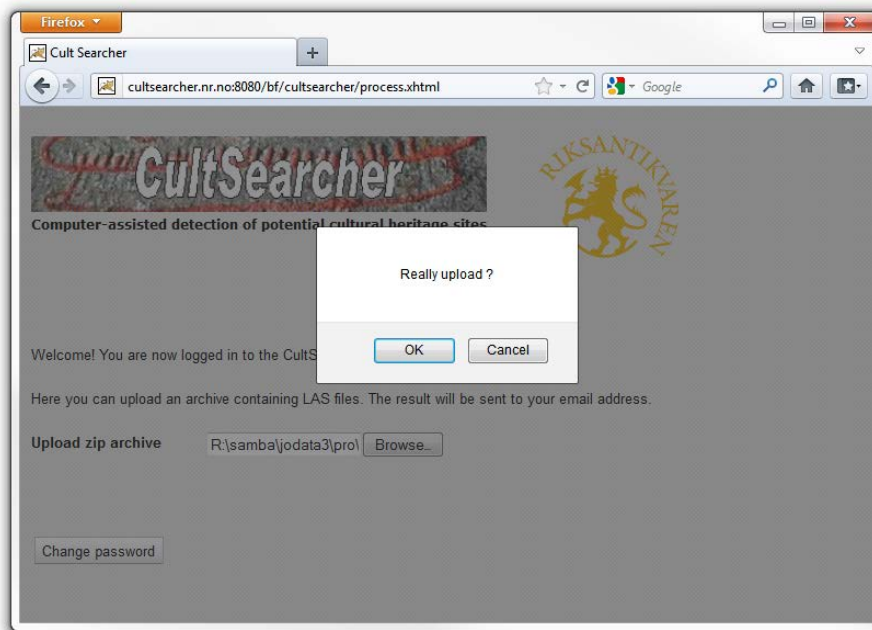
confidence level	meaning
1	very low
2	low
3	medium
4	medium high
5	high
6	very high

Now that you know what you can expect back from the CultSearcher portal, you may want to group several LAS files together in one big zip file, in order to get only one set of shape files for your entire dataset. However, the uploading may take quite some time, depending on the speed of your internet connection, so you should start with a zip file containing a single LAS file only.



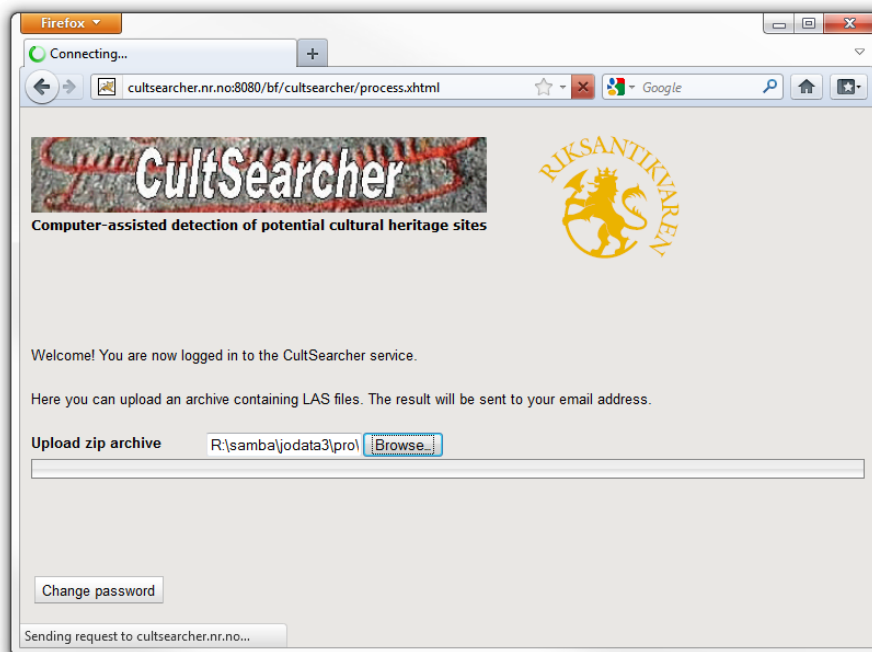
Click the browse button and locate the zip file you want to upload.

When you have selected the file, a popup window appears, with the question “really upload?”

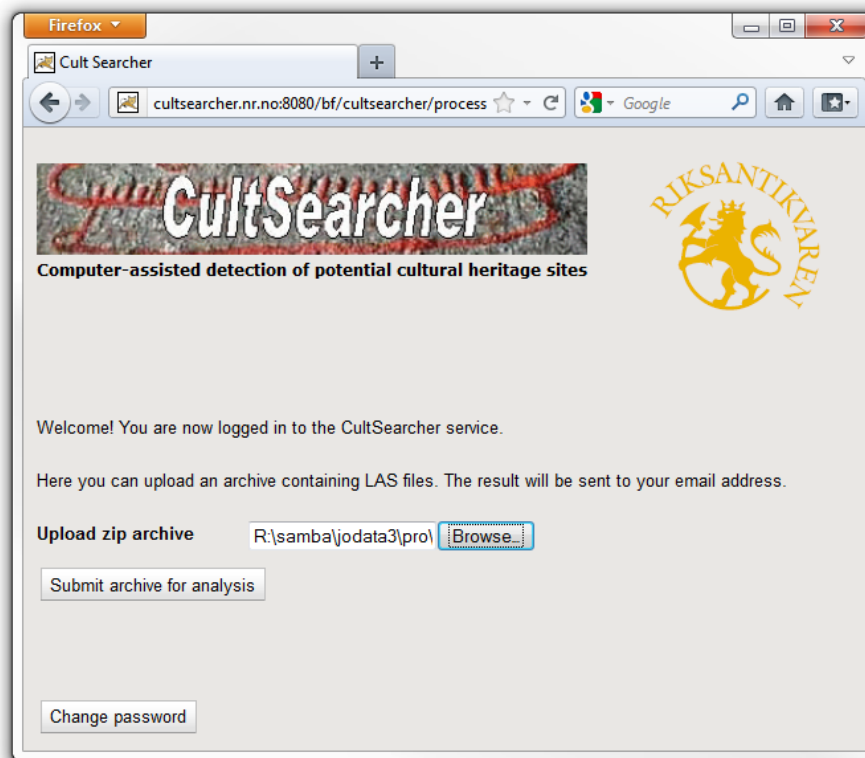


Click OK.

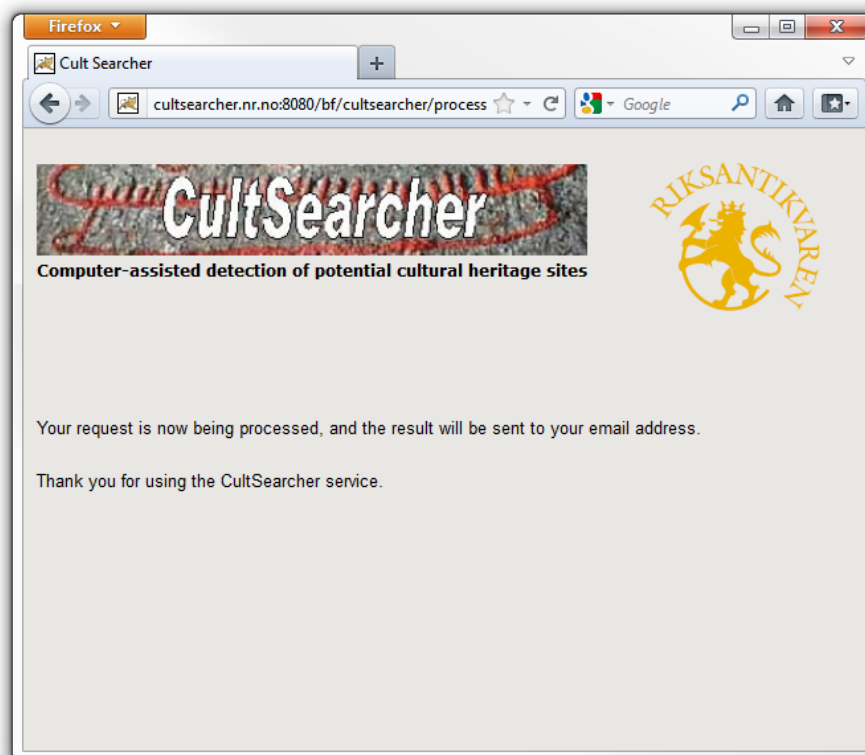
A progress bar appears below the 'browse' button.



The uploading may take some time. When finished, a new button will appear: submit archive for analysis.

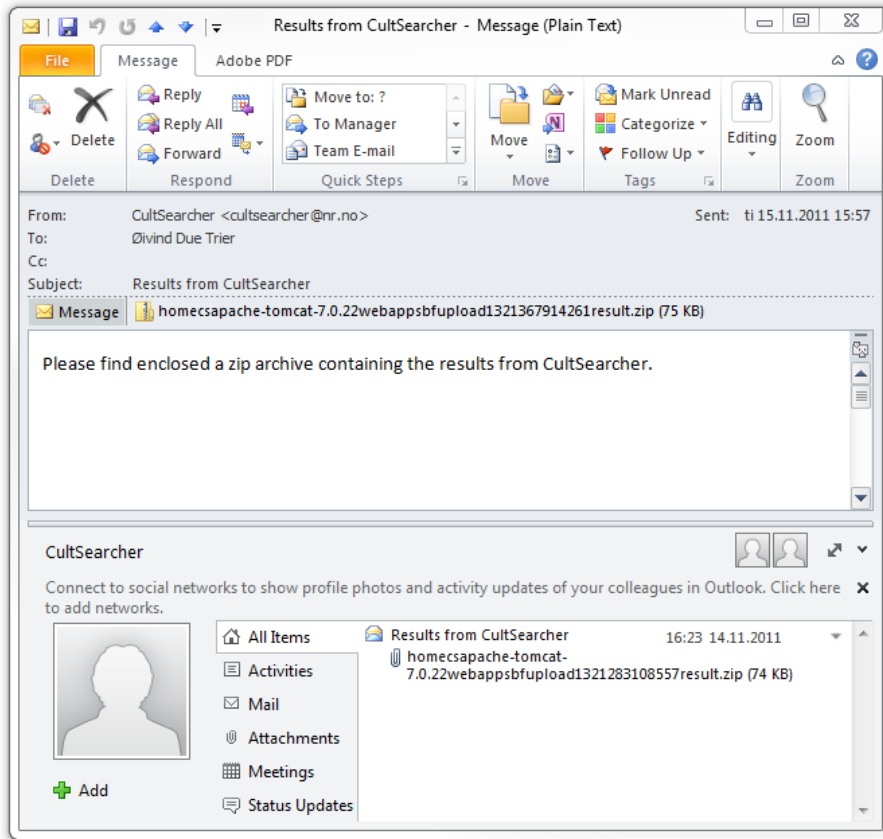


Click the button labelled 'submit archive for analysis'. Your request will now be processed.



The processing result will be emailed to you as one attachment: result.zip. This zip archive contains, for each confidence level, shp, shx and dbf files for the detections of that confidence level.

At the moment, only one request will be handled at a time, so if another request is being processed, the new request will be held in queue for up to 24 hours.



When you receive the email, it will either contain a zip file attachment with the detection results, or a message stating that the processing could not start because the pilot was busy analysing other datasets. The latter kind of message will appear after about 24 hours, during which the pilot has tried to start the processing every single hour.

## 7 Discussion and Conclusion

The project is now going into its tenth year. A major breakthrough was made in 2010. Airborne lidar data, with sufficiently high point density for archaeology to be visible in the data, were made available to the project. Some quick prototyping revealed that there was a great potential in developing an automatic pit detection method. Then, such a method was developed, and it is now being used on a regular basis by Oppland County for the mapping of hunting systems and iron extraction sites.

Initial experiments in 2011 have revealed that there is also great potential for an automatic method for the detection of heaps in the lidar data, for the purpose of mapping grave mounds in forested areas.

A drawback with the current methodology is that a number of thresholds have to be set manually, both for the classification into, say, pits versus non-pits, and for providing confidence estimates for the automatic detections. We plan to develop a statistical method that is able to estimate the confidence values without the need for manually set thresholds. For the automatic pit detection, this requires a reasonably large amount of verified archaeological pits (pitfall traps and charcoal burning pits), which can be divided into a training set and a test set. The purpose of the training data set is to automatically determine classification rules (pit vs. non-pit) and confidence estimation rules. The test set is then used to give an estimate of the performance on new data sets. We think that the Olstappen data set is sufficiently large for developing a statistical classifier, including confidence estimation, and propose to do so in 2012. If successful, we believe that the same approach should be taken for automatic heap detection.

Since Oppland County is already using the automatic detection method in the mapping of hunting systems and iron production sites, the methodology has proven that it is mature and ready for implementation in an operational web service. As described in Chapter 6, we have started to implement a pilot for such a portal. This work will continue in 2012.

One problem that is observed in the lidar data we have encountered so far, is that low vegetation cannot be separated from the ground. In order to investigate this problem, we want to collect a lidar data set with full waveform. Hopefully, it will then be possible to separate the low vegetation from the ground. The extra cost for this acquisition mode is expected to be NOK 150,000 including VAT. We hope to achieve a cost sharing through the Geovekst collaboration, so that the project's budget will cover half of the extra cost.

We are in the process of getting access to existing airborne lidar data sets from several municipalities in Vestfold and Oppland counties, and also from the city of Oslo. All these data sets have been collected with discrete returns. It will be interesting to see if the automatic detection methods can be applied to these data sets without the need for re-training of the classifiers.

## References

- Aurdal, L., Eikvil, L., Koren, H., Loska, A., 2006. Semi-automatic search for cultural heritage sites in satellite images. In *From Space to Place, Proceedings of the 2nd International Conference on Remote Sensing in Archaeology*, Rome, Italy, December 4-7, 2006, pp. 1-6.
- Bewley, R. H., Crutchley, S. P., Shell, C. A., 2005. New light on an ancient landscape: lidar survey in the Stonehenge World Heritage Site. *Antiquity* 79, pp. 636-647.
- Coluzzi, R., Masini, N., Lasaponara, R., 2010. Flights into the past: full-waveform airborne laser scanning data for archaeological investigation. *Journal of Archaeological Science*, 38 (9), pp. 2061-2070.
- Devereux, B. J., Amable, G. S., Crow, P., Cliff, A. D., 2005. The potential of airborne lidar for detection of archaeological features under woodland canopies. *Antiquity* 79, pp. 648-660.
- Devereux, B. J., Amable, G. S., Crow, P., 2008. Visualisation of lidar terrain models for archaeological feature detection. *Antiquity* 82, pp. 470-479.
- Hastie, T., Tibshirani, R., Friedman, J., 2009. *The Elements of Statistical Learning. Data Mining, Inference, and Prediction*. Second Edition. Springer: New York.
- Hesse, R., 2010. Lidar-derived local relief models – a new tool for archaeological prospection. *Archaeological Prospection* 17, pp. 67-72.
- Kokalj, Ž., Zakšek, K., Oštir, K., 2011. Application of sky-view factor for the visualisation of historic landscape features in lidar-derived relief models. *Antiquity* 85, pp. 263-273.
- Kwak, D. A., Lee, W. K., Lee, J. H., Biging, G. S., Gong, P., 2007. Detection of individual trees and estimation of tree height using lidar data. *Journal of Forest Research* 12, pp. 425-434.
- LAS specification*, version 1.3 – R11, October 24, 2011. The American Society for Photogrammetry & Remote Sensing, 18 pp. [online 2012-02-07] URL: [http://www.asprs.org/a/society/committees/standards/LAS\\_1\\_3\\_r11.pdf](http://www.asprs.org/a/society/committees/standards/LAS_1_3_r11.pdf)
- Pirotti, F., 2011. Analysis of full-waveform LiDAR data for forestry applications: a review of investigations and methods. *iForest* 4, pp. 100-106 [online 2011-06-01] URL: <http://www.sisef.it/iforest/show.php?id=562>.
- Powlesland, D., 2011. Identifying the unimaginable – managing the unmanageable. In Cowley, D. C. (Ed.), *Remote Sensing for Archaeological Heritage Management, Proceedings of the 11th EAC Heritage Management Symposium*, Reykjavik, Iceland, 25-27 March 2010. EAC Occasional Paper No. 5, pp. 17-32.
- Prokop, R.J., Reeves, A.P., 1992. A survey of moment-based techniques for unoccluded object representation and recognition. *CVGIP: Graphical Models and Image Processing* 54(5), pp. 438-460.
- Rottensteiner F., Briese C. 2002. A new method for building extraction in urban areas from high-resolution lidar data. In Proceedings of the ISPRS Technical Commission III Symposium 2002,

Photogrammetric Computer Vision, 9-13 September 2002, Graz, Austria. *International Archives of the Photogrammetry, Remote Sensing and Spatial Information Sciences*, vol. 34, no. 3A, pp. 295-301.

Sampath A., Shan J. 2010. Segmentation and reconstruction of polyhedral building roofs from aerial lidar point clouds. *IEEE Transactions on Geoscience and Remote Sensing* 48(3), pp. 1554-1567.

Somol, P., Pudil, P., Novovičová, J., Paclík, P., 1999. Adaptive floating search methods in feature selection. *Pattern Recognition Letters* 20, pp. 1157-1163.

Trier, Ø. D., Larsen, S. Ø., Solberg, R., 2009. Automatic detection of circular structures in high-resolution satellite images of agricultural land. *Archaeological Prospection* 16, pp. 1-15. DOI: 10.1002/arp.339.

Trier, Ø. D., Brun, T. A., Gustavsen, L., Loftsgarden, K., Pilø, L. H., Salberg, A.-B., Solberg, R., Stomsvik, K. H., Tønning, C., 2011. *Application of remote sensing in management of cultural heritage. Project report 2010*. Norwegian Computing Center, NR Note No. SAMBA/11/11, 139 pp.

Trier, Ø. D., Pilø, L. H., 2012. Automatic detection of pit structures in airborne laser scanning data. Submitted to *Archaeological Prospection*, October 2011; revised version submitted February 2012.

Wang, M., Tseng, Y. H., 2004. Lidar Data Segmentation and Classification Based on Octree Structure. In Proceedings of the 20th International Society for Photogrammetry and Remote Sensing (ISPRS) Congress, Commission III, 12-23 July 2004, Istanbul, Turkey.